

***In Situ* GISAXS Investigation of Low-Temperature Aging in Oriented Surfactant-Mesostructured Titania Thin Films**

Suraj Nagpure[†], *Saikat Das*[†], *Ravinder K. Garlapalli*[†], *Joseph Strzalka*[‡], and *Stephen E. Rankin*^{†,*}

[†] University of Kentucky, Chemical & Materials Engineering Department, 177 F.P. Anderson Tower, Lexington, KY 40506-0046 USA

[‡] X-Ray Science Division, Argonne National Laboratory, Argonne, IL, USA

Abstract

The mechanism of forming orthogonally oriented hexagonal close packed (o-HCP) mesostructures during aging of surfactant-templated titania thin films is elucidated using *in situ* grazing incidence small-angle x-ray scattering (GISAXS) in a controlled-environment chamber. To promote orthogonal orientation, glass slides are modified with crosslinked Pluronic P123, to provide surfaces chemically neutral towards both blocks of mesophase template P123. At 4 °C and 80% RH, the o-HCP mesophase emerges in thin (~60 nm) films by a direct disorder-to-order transition, with no intermediate ordered mesophase. The Pluronic/titania o-HCP GISAXS intensity emerges only after ~10-12 minutes, much slower than previously reported for small-molecule surfactants. The Avrami model applied to the data suggests 2D growth with nucleation at the start of the process with a half-life of 39.7 minutes for the aging time just after the induction period of 7 minutes followed by a period consistent with 1D growth kinetics. Surprisingly, films that are thicker (~250 nm) or cast on unmodified slides form o-HCP mesophase domains, but by a different mechanism (2D growth with continuous nucleation) with faster and less complete orthogonal alignment. Thus, the o-HCP mesophase is favored not only

by modifying the substrate, but also by aging at 4 °C, which is below the lower consolute temperature (LCST) of the poly(propylene oxide) block of P123. Consistent with this, *in situ* GISAXS shows that films aged at room temperature (above the LCST of the PPO block) have randomly oriented HCP mesostructure.

Keywords: self-assembly, thin films, mesophases, block copolymers, sol-gel

Introduction

The Evaporation Induced Self Assembly (EISA) process¹ is a rapid, scalable approach to preparing surfactant-templated ordered mesostructured silica films by evaporation of solvents during spin²⁻⁴ and dip coating.⁵ Because of the well-defined structure of these engineered nanostructured thin films, EISA has been adopted for a wide variety of applications⁶⁻¹⁰ including protective films¹¹⁻¹², low-k dielectrics¹³⁻¹⁵, sensors¹⁶⁻²¹, nanomaterial templates²²⁻²⁹ and membranes.³⁰⁻³⁸ Titania is of particular interest for its optical, electronic and chemical properties³⁹⁻⁴⁸ and by using highly acidic conditions, mesoporous titania films with several pore geometries have been synthesized.⁴⁹⁻⁵² However, of all possible structures, films with hexagonally close packed pores oriented orthogonal to the film (o-HCP architecture) are desirable because they provide an accessible array of nonintersecting channels for rapid transport of reactants or charge carriers,⁵³⁻⁵⁸ for creating devices with confinement-induced properties,⁵⁹⁻⁶³ and for templating of nanowire arrays.⁶⁴⁻⁶⁸ Related orthogonally oriented TiO₂ nanotube arrays prepared by anodizing titanium⁶⁹ have been used to demonstrate some of these advantages,⁷⁰⁻⁷⁵ but contain relatively large pores (>25 nm diameter) and do not have the processing flexibility provided by the EISA method. TiO₂ films with bicontinuous cubic pores also provide accessible, nm-scale pores without requiring special alignment procedures,^{52,76} but interconnected pores are not desired for some applications. Also, with some templates, cubic films form over narrow composition ranges⁷⁷ and are fragile because of their high porosity.

By analogy with surface chemistry strategies used to orient block copolymer films,⁷⁸⁻⁸³ the Rankin group has reported the synthesis of mesoporous titania thin films with o-HCP cylindrical nanopores using EISA with P123 (a triblock copolymer with composition HO(CH₂CH₂O)_x(CH₂CH(CH₃)O)_y(CH₂CH₂O)_xH, where on average $x = 20$ and $y = 70$) as

structure directing agent and titanium(IV) ethoxide as titania precursor.⁸⁴⁻⁸⁵ The hypothesis underlying this approach is that orthogonal alignment of the HCP mesophase can be achieved in a EISA-derived ceramic film by modifying the substrate surface so that it interacts equally with both blocks of the P123 template, making it chemically “neutral” towards the template surfactant. Monte Carlo simulations⁸⁶⁻⁸⁷ have shown that this is the expected outcome for mixtures of surfactants and small molecules, and not just for neat block copolymers⁸². A related epitaxial orientation procedure was demonstrated by Tolbert and coworkers, where HCP film was cast onto a cubic template film to induce orthogonal alignment.⁸⁸ In addition to surface modification, the synthesis procedure for o-HCP TiO₂ films includes aging after coating in a refrigerator at 4 °C under high relative humidity (approx. 94%). The objectives of using a low temperature are to slow titanium precursor condensation and to provide a driving force for mesophase formation, similar to the subambient temperatures used by Alberius et al.⁷⁷ Even though this aging procedure has been found to be an essential part of o-HCP TiO₂ film formation, little is known about the o-HCP mesostructure formation mechanism other than what has been inferred by characterization of the films before and after calcination.⁸⁵

To understand the mesostructure evolution of thin films during EISA, several groups have used a wide range of techniques including grazing incidence small angle x-ray scattering (GISAXS), transmission electron microscopy and time resolved Fourier transform infrared spectroscopy (FTIR).⁸⁹⁻¹⁰⁰ Among these techniques, GISAXS is most relevant here because it can be conducted *in situ*, and it provides insight into mesostructure development and organization during the formation of self-assembled particles¹⁰¹ and EISA thin films⁹⁸. Grosso et al. analyzed the mechanisms involved in the formation of 2D-hexagonal templated SiO₂ and TiO₂ mesostructured films during dip coating using Brij-58 as surfactant and found that the self-

assembly leads to the formation of organized phase at the final stage of the drying process and involves the formation of an intermediate disorganized phase.⁹⁴ The disorder to order transition takes place within 2-3 minutes after the start of coating for TiO₂ and SiO₂ under the conditions studied. Other reports have shown that for dip-coated thin films, the mesostructure generally forms through a disorder-to-order transition which may involve intermediate hybrid mesophases that are related to the concentration gradient.^{90-91,102} Doshi et al. studied the self-assembly of surfactant template thin-film silica mesophases synthesized using surfactants cetyltrimethylammonium bromide (CTAB) and Brij-56 and found that 2D HCP mesostructure (*p6mm*) forms from a lamellar mesophase through a correlated micellar intermediate.⁹² Gibaud et al. studied EISA of silica mesophases synthesized using surfactant CTAB and found that the final structure of the film is strongly influenced by the rate of evaporation which itself governs the concentration gradient inside the film.⁹³ While *in situ* SAXS studies of EISA have provided magnificent insights, most have been restricted to the dip-coating process itself and the time span on the order of seconds after the coating process. Also, most of the studies have been done for mesoporous silica films synthesized with small surfactant molecules (CTAB and Brij surfactants) and very few studies have been done for TiO₂ films. Thus, it is not known to what extent their findings can be extrapolated to the conditions used to synthesize o-HCP films.

One surprising finding for o-HCP TiO₂ films is that, while most prior *in situ* GISAXS studies of EISA suggest that the final mesostructure forms during (or within seconds after) dip coating, mesophase orientation can be controlled by sandwiching ~250 nm thick films with a second chemically neutral slide well after the coating process is complete (on the order of up to 20 minutes).^{84,103} However, this type of post-coating modification is not unprecedented; as Grosso and coworkers discuss in reviews of the fundamentals of mesostructuring through EISA,

a tunable steady state (TSS) occurs in some cases, during which the inorganic framework is still flexible and susceptible to modification by changing aging conditions.^{10,95} The TSS helps to explain why the structure of EISA-derived films can be tuned by adjusting variables such as the humidity of the vapor,¹⁰⁴⁻¹⁰⁶ the sol aging time (which affects the time scale for condensation after coating),¹⁰⁶⁻¹⁰⁷ the pH of the film,¹⁰⁸⁻¹¹⁰ the presence of solvent vapors,¹¹¹ and confining the coating using materials of different surface energy.^{84,103,112-114} Generally for silica, this TSS lasts from a few seconds at low humidity to 10 minutes at high humidity.¹¹⁵ However, for TiO₂ system, the condensation of titania oligomers has been proposed to be triggered by evaporation of HCl. Because HCl departs very slowly, TSS for some TiO₂ sol compositions of more than 1 hour duration have been observed.⁹⁵ Because the TSS plays an important role in the formation of o-HCP TiO₂ films, studying the process *in situ* will provide novel insights into how to engineer and tune EISA films for new applications requiring an active oxide component.

Here, *in situ* GISAXS is used to monitor the formation of the o-HCP mesophase in P123 templated TiO₂ films during a relatively long time frame as the films age (which corresponds to the TSS). The objective is to directly test the hypothesis that o-HCP structure develops during film formation due to modification of the surface with crosslinked P123.⁸⁴⁻⁸⁵ A possible alternative hypothesis is that the o-HCP structure emerges via anisotropic merging of pores in a precursor Im $\bar{3}$ m phase, which has been observed by other researchers in TiO₂ films with accessible vertical pores.^{95,116-117} The measurements will be made using a linear actuator enclosed in a controlled-environment chamber to withdraw a coated film and to monitor its evolution by GISAXS during aging. Results will be compared for thin (~60 nm) films on modified and unmodified glass surfaces, thicker films, and as a function of aging temperature.

The kinetics of the mesostructure evolution will be modeled using the Avrami equation and will be compared to relevant o-HCP structures in block copolymer films.

Experimental Section

NoChromix powder (Godax Laboratories, Inc.), concentrated sulfuric acid (95-98%, Sigma Aldrich), P123 (poly(ethylene glycol)-block-poly(propylene glycol)-block-poly(ethylene glycol) with $M_n \sim 5800$, Sigma-Aldrich), 1,6-diisocyanatohexane (98%, Sigma Aldrich), glycerol (99+%, Sigma Aldrich), titanium ethoxide (Technical grade, Sigma Aldrich), HCl (36 wt%, EMD Chemicals), ethanol (200 Proof, Decon Laboratories) and acetone (Fisher Scientific) were all used as received.

The sol required for titania film synthesis was prepared based on the procedures of Koganti et al.⁸⁴ Prior to depositing any material, borosilicate glass slides (1 in \times 2 in) were cleaned with a NoChromix glass cleaning solution in sulfuric acid prepared according to the manufacturer's instructions. To modify slides with crosslinked P123 (when this was done), cleaned glass slides were dip coated using an acetone-based solution containing equimolar amounts (0.415 mM) of Pluronic surfactant P123 and 1,6-diisocyanatohexane. To this solution, a single drop of glycerol was added to serve as a cross-linker so that the films would be stable. The slides with modifying coating were aged at 120 °C overnight to drive the cross-linking reaction to completion. The thickness of cross-linked P123 as measured using profilometry was ~ 30 nm with surface roughness of 4-5 nm. This cross-linked P123 layer is expected to be removed completely after calcination at 400 °C as shown previously.⁸⁵ Titania sols were prepared by adding 2.1 g of titanium ethoxide to 1.53 g concentrated HCl, stirring for 10 min and adding 0.65 g of P123 dissolved in variable amount of ethanol. 32 g of ethanol was used for thin films and 6 g for thick films.

In situ aging GISAXS experiments were done at the Advanced Photon Source (APS) at Argonne National Labs on beamline 8-ID-E using an x-ray beam $100\ \mu\text{m}$ (H) \times $50\ \mu\text{m}$ (V) with wavelength of $1.6868\ \text{\AA}$.¹¹⁸ The APS operated in top-up mode, i.e. at constant storage ring current, during the measurements. Fig. 1 shows the chamber and scattering geometry for *in situ* GISAXS experiment. Samples for *in situ* dip coating were prepared within a sealed chamber with inner dimensions $5 \times 5 \times 6.5\ \text{in}^3$ with aluminum side walls and copper lid and base plate. Unless otherwise noted, the base plate was in thermal contact with a circulating chiller maintained at $4\ ^\circ\text{C}$. Helium gas bubbled through saturated potassium sulfate solution into the chamber to maintain constant relative humidity. A digital hygrometer (VWR model 35519-050) with probe inserted in the lid monitored the relative humidity inside the chamber, typically $\text{RH} > 80\%$. The sol prepared as explained above was contained in a plastic container, (the lid of a 50 mL Falcon tube) approximately 10 mm deep, resting on a copper block in thermal contact with a thermoelectric element so that its temperature could be changed independently. A small translation stage raised a glass slide out of the solution at about 15 mm/min. X-rays entered the chamber through a mica window and were incident on the sample several mm above the surface of the solution. Scattered x-rays exited the chamber through a Kapton window. Unlike the usual scattering geometry for GISAXS at Beamline 8-ID-E, the vertical sample meant the scattering plane was horizontal with the phi-circle of the diffractometer controlling the incident angle. A small piece of tungsten, $1 \times 2 \times 15\ \text{mm}^3$ attached horizontally to the end of the GISAXS beamstop served as the beamstop for the *in situ* dip coating GISAXS measurements. The distance from the sample to the detector (Pilatus 1M, Dectris) was 1474 mm. The analysis of the GISAXS data was done using the GIXSGUI package for Matlab.¹¹⁹ Consideration of the

scattering geometry shows that corrections for the instrumental resolution are negligible compared to the experimentally observed peak widths described below.¹²⁰

To understand the effect of aging temperature on mesostructure development and orientation, scanning electron microscopy (SEM) was performed using a Hitachi S-4300 at 3 kV. The films after *in situ* GISAXS were calcined in a muffle furnace (Vulcan 3-550) at 400° C for 10 minutes after heating at a ramp rate of 25° C/min followed by rapid cooling. SEM samples were prepared by cutting the glass slide to the desired shape using a glass cutter and then mounting exactly at the center of an SEM stub coated with carbon tape. The edges of the sample were coated with colloidal graphite (isopropanol base) to increase conductivity by keeping the top surface in electrical contact with the lower surface. SEM samples were aged at 120° C overnight (~12 h).

Results and Discussion

The thickness of the thin titania films in this study (prepared using 32 g of ethanol) was determined by ellipsometry to be ~60 nm after aging, which has previously been found to be thin enough to give orthogonally oriented pores without sandwiching the films with a second neutral surface.^{84,103} *In situ* GISAXS patterns were recorded for this sample in intervals of 1 minute from the start of the aging process until 30 minutes of aging time at one spot on the film, located 13.5 mm above the bottom of the coated section. The sampling geometry of the sampling is shown schematically in **Figure 1** and described in more detail in the Experimental Section. After this period, patterns were collected with the beam at this spot and four additional spots to determine spot-to-spot variability and to test for beam damage, at 45 min, 60 min and 75 min of aging. **Figure 2** shows selected 2D GISAXS patterns at representative times during the evolution of the mesostructure for a thin titania film on modified substrate during aging at 4 °C. Generally the presence of the o-HCP cylindrical mesophase is indicated by two intense rods parallel to the

scattered beam, located on both sides of the beam stop. These rods can be indexed to the (100) plane of the HCP structure and their rod shape can be attributed to the finite cylindrical shape of the micelles (Kiessig fringes are most likely not observed because of a distribution of rod lengths and orientations).⁸⁵ The GISAXS patterns show that in the first 10 minutes of aging (Fig. 2a), there is no indication of mesostructure development as we do not see any spots or rods in the pattern. After 15 minutes (Fig. 2b), faint spots can be seen on both sides of the beam stop due to diffraction in the plane of the film, which indicates that mesostructure started developing even though it is still not well defined. After 20 minutes of aging (Fig. 2c), clear vertical rods are visible on both sides of the beam stop indicating that the orthogonally oriented cylindrical micelles started developing. The intensity of the vertical rods further increases for longer aging times (for example, the pattern at 75 min, Fig. 2d).

While only selected time points are shown in Fig. 2, no distinct out-of-plane diffraction spots (which indicate parallel alignment of micelles or a mesophase with 3D symmetry) are visible at any other time points. Other studies that showed the formation of vertically oriented cylindrical channels by transformation of a cubic phase and merging of the pores normal to the film also showed diffraction spots consistent with the cubic phase prior to thermal treatment.^{52,116-117} The absence of out-of-plane diffraction spots is consistent with the hypothesis underlying the work of Koganti et al.⁸⁴ that vertical channels simply form due to reorientation of the HCP phase in response to the modification of the surface of the substrate with a chemically neutral crosslinked P123 layer. The o-HCP structure is the first ordered mesophase formed, and it emerges slowly by a disorder-order transition consistent with the TSS proposed for highly acidic TiO₂ sols.^{10,95} The slow mesophase formation and long TSS may also be accentuated by the use of P123 as a template.¹²¹

Many more GISAXS patterns were collected than those shown in Fig. 2, but it is not easy to discern the quantitative variation in the intensity of the (100) rods by direct inspection of the 2D patterns. Therefore, linecuts were generated by integrating the 2D patterns for q_z values covering the Yoneda band from 0.025 to 0.03 \AA^{-1} . **Figure S11a** (Supporting Information) shows a representative 2D GISAXS pattern along with the region of integration for the linecut shown using vertical lines. The resulting linecut is shown in **Figure S11b** on a semilog scale. The high intensity peaks at $q_y = \pm 0.0425 \text{\AA}^{-1}$ are the orthogonally oriented (100) diffraction peaks. Note that the beamstop was asymmetrically positioned to optimize the view at low q_y values on the positive side of the beamstop (a gap in the CCD array was positioned to the left of the beamstop).

Figure 3 shows a waterfall plot illustrating the evolution of the 1D linecut patterns on a log-log scale for a thin titania film on modified substrate during aging at 4 °C and ~80% RH. The Yoneda band includes a shoulder at low q_y values whose intensity increases for the first 10 minutes and then reaches a plateau with very little change afterwards, either in amplitude (see Supporting Information **Figure S12a**) or position (**Figure S12b**). The growth of this shoulder shows that there is no indication of beam damage to the sample prior to mesostructure development. For the first few minutes of aging, the intensity of the (100) diffraction peak is very low, indicating that the development of an ordered mesostructure has not begun. After an induction period on the order of several minutes, (100) diffraction peaks appear symmetrically and grow in intensity until 25 minutes of aging. However, after 25 min, the intensity of the peak decreases until the end of the 30 min initial kinetic period (see below). Throughout the kinetic measurement, the shape of the diffraction pattern and the position of (100) diffraction peak does not change significantly, indicating growth of a mesophase with constant structure. A similar

disorder-to-order transition was reported during the formation of vertically oriented cylindrical block copolymer mesophases during solvent annealing¹²² and thermal treatment,¹²³ although detailed kinetics were not reported. To quantify the kinetics in the present case, the integrated intensity of the (100) peak in the linecuts (after baseline correction) was used as a measure of the extent of development of the o-HCP phase with respect to time during aging.

Figure 4a shows the evolution of o-HCP ordering in a thin film on modified substrate during aging at 4 °C. The measured integrated intensity at a fixed position (13.5 mm above the bottom of the slide) is shown with filled circles starting from 1 minute to 75 minutes of aging. The trend in these detailed data is consistent with the qualitative description of Fig. 2. The intensity initially is close to zero, and increases little for the first 7 minutes of aging. The mesophase transformation then accelerates in accordance with a disorder-order transition, with a maximum rate of intensity increase at about 16 minutes, and continued slow mesostructure development up to 25 minutes. The intensity then decreases somewhat for the remainder of the period of frequent GISAXS scanning. This most likely is a result of accumulated radiation damage due to frequent exposure of the same spot on the sample to the high intensity x-ray beam. Note that this is the first and only indication of beam damage during sampling and suggests only mild deformation of the long-range order of an assembling mesostructure since P123 mesophases in water melt at temperatures ranging from 45 to 85 °C.¹²⁴ We attribute this accumulated radiation damage to the kinetics / thermal effect described previously by Malfatti et al.¹²⁵ during mesophase transitions. Consistent with this explanation, the intensity increases again at later times, when the frequency of scanning decreases. This shows that the damage is reversible, although the extent of reversibility is limited by ongoing polycondensation of titania.

The increase in intensity is accompanied by a decrease in the width of the peak consistent with continuous mesophase nucleation and growth (see below).

Varying the vertical position of the sample allowed us to measure fresh parts of the sample that were not exposed to the x-ray beam during the earlier time series (at $z = 13, 13.3, 14$ and 14.2 mm, as compared to $z = 13.5$ mm for the initial time series. Note that the vertical size of the beam was 0.05 mm). The patterns obtained were qualitatively the same, only differing in the intensity of the features, indicating that the material curing away from the beam evolves to the same structure as the part of the sample where the evolution was observed with the series of x-ray exposures at short times. Performing similar integrations and plotting the intensities shows that the intensity can be smoothly interpolated between the initial part of the time-resolved series at small t ($t < 25$ minutes) and the intensity from fresh regions of the sample at later times (open symbols in Figure 4a). From this study, it appears that 45 minutes is the minimum aging time to develop the o-HCP mesostructure close to its full extent at 4 °C.

To understand the role of surface modification in the development of the o-HCP mesostructure, a GISAXS study was conducted during aging at 4 °C for a thin titania film on unmodified substrate. According to the hypothesized effect of the substrate surface chemistry, this would have been expected to give out of plane diffraction consistent with the HCP mesophase oriented parallel to the glass slide. Instead, the same type of pattern developed as in Fig. 2, corresponding to an o-HCP mesophase. This surprising result indicates that the orthogonal orientation is promoted not only by the surface modification, but also by the temperature and humidity of the system during aging. Unlike prior studies in which the films were coated at room temperature and then transferred to a refrigerator for aging,⁸⁴⁻⁸⁵ here the films were coated and aged at the same low temperature. This is significant because of the

temperature-dependent behavior of P123. A comprehensive study of Pluronic surfactants (triblock copolymers of poly(ethylene oxide)-b-poly(propylene oxide)-b-poly(ethylene oxide) (EO_xPO_yEO_x) in water by Wanka et al.¹²⁴ showed that significant thermotropic behavior occurs in Pluronics because of changes in the solubility of the poly(propylene oxide) (PPO) blocks. In a temperature range from 15-20 °C, P123/water mixtures were reported to transition from ordered mesophase (at high temperature) to isotropic mixtures and from micelles to dissolved monomers (depending on the concentration).¹²⁴ Thus, at 4 °C, the contrast in hydrophilicity between PPO and poly(ethylene oxide) (PEO) is reduced and the polymer may find hydrophilic surfaces to be "neutral". However, the titanate species mixed with the PEO blocks still provide sufficient driving force for mesophase formation by increasing the Flory-Huggins interaction parameter of the system leading to microphase separation,¹²⁶ as a result of which orthogonal alignment of the cylindrical micelles occurred on an unmodified substrate also. The high relative humidity during aging may also contribute to the orthogonal alignment; a recent self-consistent field study by Fredrickson and coworkers showed that orthogonal cylinders are favored by slow evaporation and weak block segregation when a good solvent for both blocks is used.¹²⁷ This contradicts the trend in many solvent-annealed block copolymer hexagonal films, but the solvent used for annealing usually has a strong preference for one block.¹²⁸ Here, both volatile species (ethanol and water) are good solvents for PEO and PPO at 4 °C, so slow evaporation due to the low temperature and high RH are expected to favor the o-HCP phase.

Figure 4b shows the evolution of the intensity of the (100) peak on unmodified substrate during aging at 4 °C at 13.5 mm above the bottom of the slide, along with the average intensity curve with the error bars as standard deviation. The same procedure was followed as for the film on modified substrate for measurement and analysis. In the beginning, the mesostructure

development takes place more rapidly as compared to the film on modified glass. However, the values for average maximum intensity at steady state are lower than those observed for the modified substrate. The maximum average intensity for unmodified substrate is 0.34 ± 0.066 which is half as compared to the average maximum intensity of 0.68 ± 0.073 for the film on a modified substrate. This large difference in intensity indicates that even though vertical alignment of cylindrical micelles occurs for unmodified substrate after aging at $4\text{ }^{\circ}\text{C}$, it is only partial; a larger amount of material with well-ordered o-HCP domains is found with glass modification.

Because a contrast in orientability has been found in the past between thin films ($<100\text{ nm}$) and thicker films, thick films (thickness $\sim 250\text{ nm}$) were also studied by GISAXS by preparing films with less ethanol (6 g). According to Koganti et al.,⁸⁴ for thick films, complete orthogonal HCP orientation is best achieved by sandwiching the films between two modified surfaces. This sandwiching is thought to be necessary because the orthogonal orientation from one modified surface does not propagate across the entire film. Thin films are advantageous because they do not need to be sandwiched between two modified surfaces in order to fully orient the HCP phase orthogonal to the substrate. **Figures 4c and d** shows the evolution of the (100) Bragg rod of thick films on modified and unmodified substrates, respectively, during aging at $4\text{ }^{\circ}\text{C}$ at a fixed position (13.5 mm above the bottom of the coating) along with the average intensity at four other positions at later times where error bars represent standard deviations among those four points. For thick films, orthogonal domains were observed even without sandwiching them between two modified surfaces (sandwiched films were not studied here due to difficulty focusing the beam on a sandwiched film). However, the average maximum intensity observed was significantly lower than for the thin film on modified substrate, which indicates

that the degree of o-HCP mesophase formation is less. While this is surprising (again) relative to prior observations of the effects of film thickness,⁸⁴⁻⁸⁵ coating and aging the films at 4 °C from the outset may have favored the o-HCP structure due to weak segregation between PPO and PEO and slow evaporation of ethanol and water.¹²⁷

Evolution of the sample structure is also evident in the changing width of the diffraction peak. **Figure 5** shows the full width at half maximum (FWHM) of the (100) peak for different titania films at 13.5 mm above the bottom of the coating or at a set of four other points (averaged). The error bars represent the standard deviation of the FWHM of the four points excluding the measurement at 13.5 mm. The FWHM for the thin titania film on modified substrate (Fig. 5a) changes continuously during the aging process, as does the size of ordered domains.¹²⁰ Scherer grain-size analysis can estimate the average number of layers contributing to the diffraction peak, $N = q_{hkl} / \Delta q_{hkl}$.¹²⁰ When the peak first appears, $N < 2$, then increases to $N \sim 8$ as FWHM decreases over the first 25 minutes of aging. The narrowing of the peak corresponds to the increase in intensity in Fig. 4a, suggesting that both nucleation and growth of ordered domains occurs during the first 25 minutes of aging. After 25 minutes, the FWHM begins increasing as the (100) intensity decreases. Correspondingly, N decreases, probably due to radiation damage, and then returns to $N \sim 8$ when the scanning frequency decreases. All of the other titania films follow the same trends as in Fig. 4 (Figs. 5b-d). The average FWHM values for the films was estimated using four spots not subject to high-frequency sampling and are shown in Fig. 5 by unfilled diamonds. The mean FWHM is generally smaller for the thin titania film on modified substrate relative to unmodified and thicker substrates, although the only statistically significant difference is between the thin film on modified substrate and the thick film on unmodified substrate.

Further quantitative insight into the kinetics of mesostructure development was gained by fitting the (100) peak intensity vs. time data to the *Kolmogorov-Johnson-Mehl-Avrami (KJMA)* model, more simply known as the Avrami equation.¹²⁹⁻¹³² The Avrami equation is used to understand the kinetics of phase transformation when nucleation and growth give rise to a sigmoidal curve. The kinetic curves shown in Fig. 4 for all films during aging at 4 °C have a sigmoidal form, so the KJMA equation was applied. The simplest form of the Avrami equation is

$$f(t) = 1 - \exp(-kt^n) \quad (1)$$

where $f(t)$ is fraction of transformation that has happened at time t , k is the rate coefficient and n is the Avrami index. This form of the Avrami equation was derived assuming that (a) nucleation occurs randomly and homogeneously over the entire untransformed portion of the material, (b) the growth rate does not depend on the extent of transformation, and (c) growth occurs at the same rate in all directions consistent with the dimensionality implied by the Avrami index.¹³³

The Avrami equation in linearized form is rewritten as:

$$\ln \left[\ln \left(\frac{1}{1-f(t)} \right) \right] = \ln(k) + n \ln(t) \quad (2)$$

Eq. 2 allows us to determine constants n and k from by linear regression from a plot of $\ln[\ln(1/(1-f(t)))]$ vs. $\ln(t)$. If the transformation follows the Avrami equation, the data on this plot should follow a single straight line for a given set of conditions. In our case, the value of $f(t)$ has been calculated by dividing the actual intensity of the (100) diffraction by the maximum average intensity observed. For example, the average maximum intensity for a thin titania film on modified substrate (Fig. 4a) was approximately 0.68 using the value obtained at large time from freshly exposed regions of the sample in order to remove the effects of radiation damage late in the kinetics of transformation. The intensity of the diffraction peak depends on the electron

density contrast between the titania walls and the mesophase, which may be influenced by the degree of polycondensation of the mesophase. However, the polycondensation rate of the inorganic matrix is not expected to be significantly affected by film thickness or surface modification. Therefore, any effects of polycondensation on the Avrami parameters should be consistent between samples at a given temperature.

Figure 6 shows the Avrami equation fit for the evolution of each of the titania films during aging at 4 °C. For each sample, a straight line was observed for the filled symbols, indicating that the Avrami equation could be applied over this range of times. However, the unfilled data points did not follow the Avrami equation. The early data (before ~7 minutes for the thin film on modified substrate during aging at 4 °C) represent an induction period during which formation of the micelles is likely to be occurring¹³⁴ (indicated by the increase in scattered intensity at low angles,¹³⁵ Fig. SI2(a)) but not giving rise to noticeable diffraction. Once sufficient radiation damage accumulated in the samples (e.g. after 25 min for thin film on modified substrate), a net decrease in $f(t)$ was observed and the Avrami equation was no longer applied.

Table 1 summarizes the Avrami equation parameters found for each of the titania films. The induction time is highest for the thin film on modified substrate (7 min) as compared to all other films (3 min), which indicates relatively slow mesostructure growth in this sample. This can also be seen from Fig. 4 where the thin film on modified substrate has a longer low-intensity initial period. We can clearly see from figure 6a that for thin film on modified substrate, there are two distinct linear regions over which the Avrami equation can be applied. The first is for aging times between 8 to 14 minutes and the other one from 16 to 25 minutes. The value of n in the Avrami equation reflects the nature of transformation and is associated with the mechanism of

crystal growth. An Avrami index of 3 is usually interpreted as three-dimensional growth of nuclei formed instantaneously or two-dimensional growth with a constant nucleation rate, whereas an Avrami index of 2 is interpreted as two-dimensional growth with nucleation at the start of the process.¹³⁶⁻¹³⁷ The value of n in Table 1 is approximately 2 (within the estimated uncertainty) for the titania thin film on modified substrate until 14 minutes of aging which is interpreted as two-dimensional growth with nucleation at the start of the process. An Avrami index of value 1 might indicate one dimensional growth for later (16-25 min) aging times for titania thin film on modified substrate. The value of the Avrami index for the thin film on unmodified substrate is calculated to be 3, which indicates two-dimensional growth with a constant nucleation rate since the films are confined in one dimension and the o-HCP phase would be expected to grow laterally in the plane of the films. Thus there is a clear difference in mesostructure growth mechanism for thin films on modified and unmodified substrate. This may be because a better oriented mesophase on modified substrate requires nucleation during the transformation process, whereas less oriented mesophase for thin film on unmodified substrate grows throughout the film from randomly oriented nuclei present at the end of the micelle formation process. The values of the Avrami index for thicker films are estimated to be 3, indicating two-dimensional growth with constant nucleation rate. The rate constant k for different films can be calculated from the y-intercept of the Avrami fit. Direct comparison of rate constants might be misleading, as they have different units. However, the kinetics of different films can be compared by calculating the half-life ($t_{1/2}$) for different films. In this case $t_{1/2}$ will be defined as the time required for the mesostructured development to evolve to half of its final value ($f(t) = 0.5$ at $t_{1/2}$). Half-life can be calculated from Eq. 2 as:

$$t_{1/2} = \left(\frac{\ln 2}{k} \right)^{1/n} \quad (3)$$

Table 1 summarizes half-lives for different titania films. For thin titania film on modified substrate, the half-life (39.7 min for parameters found during aging between 8 to 14 min and 24.7 min for aging between 16 to 25 min) is higher than for the thin film on unmodified substrate, which further indicates that the transformation is slower for the thin film on modified substrate. The half-lives for thick films on both modified and unmodified substrates are also comparable to the value for thin films on unmodified substrates. However, the maximum average intensity is highest for the thin film on modified substrate ($\sim 0.68 \pm 0.073$), which indicates that even though the evolution of orthogonal orientation is slower for thin film on modified substrate, it is the most complete and well-defined for these films. In fact, hindered diffusion of micelles (or surfactants) in a well-oriented thin film is most likely responsible for the relatively slow kinetics of mesostructure development for the thin film on modified substrate. Films which are not as well oriented show faster evolution of the phase, whether the cause is the thickness of the film or the surface chemistry.¹³⁶⁻¹³⁷

To verify the hypothesis that orthogonal orientation is favored (even in thin films on unmodified substrates or thick films) by aging at 4 °C due to weak segregation between PEO and PPO and slow solvent evaporation, GISAXS studies were also performed at room temperature (23 °C). The relative humidity in the aging chamber was in the range of 90-95% during these measurements. **Figure 7** shows selected 2D GISAXS patterns showing how the mesostructure of thin titania film on modified substrates evolves during aging at 23 °C. Here, no evidence of correlated scattering is observed during the first 5 min of aging (Fig. 7a). After 8 min of aging (Fig. 7b), a diffuse ring pattern appears surrounding the beam stop and scattered beam. The intensity of the diffuse ring further increases and it becomes more distinct with increasing aging time (Fig. 7c/d). However, unlike all of the patterns collected at 4 °C, no rods suggesting in-

plane diffraction were observed at any point in the aging process. Instead, the diffuse ring indicates that randomly oriented HCP domains form in the films, with no preferred orientation.

To confirm and to better understand the effects of aging temperature on mesostructure orientation, *ex situ* SEM characterization was done. The samples used for *in situ* GISAXS were calcined at 400 °C for 10 minutes after heating at a rate of 25 °C/min. **Figures 8a and 8c** show representative SEM images for P123-templated titania thin films aged on modified substrates aged at 4 °C and 23 °C, respectively. For the film aging at 4 °C (Fig. 8a), a very well-ordered, accessible porous structure was observed everywhere indicating vertical alignment of the cylindrical micelles, which is consistent with the corresponding 2D GISAXS pattern collected after 30 minutes of aging (Fig. 8b), which shows (100) diffraction peak on either sides of the beam stop. When a film of the same composition deposited onto the same type of modified slide was aged at 23 °C (Fig. 8c), randomly oriented parallel stripes were observed everywhere at the top surface of the film, indicating that the cylindrical micelles were arranged parallel to the substrate but with no preferred in-plane orientation. To verify that the difference is not caused by a change in adhesion of the titania film due to removal of the organic layer during calcination, a low magnification plan view SEM image (Supporting Information Figure SI3) shows no cracks or defects in the film on modified substrate. Also, x-cut adhesion (ASTM standard D3359) ratings of 4A (out of 5) were measured for films with and without the crosslinked P123 layer, revealing no difference in adhesion. From the 2D GISAXS pattern collected after 30 min of aging (Fig. 8d), it is clear that the overall mesostructure during aging at 23 °C has random orientation throughout the film, but with some degree of parallel orientation near the film surface (Fig. 8c). This suggests that there may be a gradient in the mean orientation of the micelle domains, with domains near the surface aligned parallel to the substrate, domains near the thin

film/substrate interface oriented orthogonal to the substrate, and domains in the interior of the thin film randomly oriented, combining so that overall a powder diffraction ring is obtained due to the range of orientations of the HCP domains.

In order to test this hypothesis, SEM images were collected of the base of the films (at the film / substrate interface). To do this, one side of a glass slide was covered with masking tape after cleaning. Both sides were coated with the crosslinking P123 solution and cured, and then both sides were coated with titania sol and aged for 2 h in the refrigerator (4 °C) or at room temperature (23 °C). Before calcining as usual, the tape from one side was peeled off and remounted upside down on another glass slide. The tape was completely removed during calcination, thus allowing the underside of the coating to be visualized. The plan view SEM images (**Figure SI4**) show that for the film aging at 23 °C (Fig. SI4a), the mesostructure at the underside of the film consists of poorly ordered accessible pores consistent with local orthogonal orientation. In contrast, the film aged at 4 °C (Fig. SI4b) exhibits ordered, accessible mesopores indicating orthogonal orientation throughout the film. This additional SEM characterization is consistent with random average orientation of the HCP mesophase throughout films aged at 23 °C, but domains predominantly parallel to the film/vapor interface and orthogonal to the film/substrate interface. This type of mixed orientation has been predicted in mesoscopic simulations of surfactants confined between flat surfaces with significantly dissimilar interactions with the mesophase components.¹³⁸

As suggested above, the reason for the difference in orthogonally oriented domains for films aged at 4 °C and 23 °C might have to do with the temperature dependence of hydrophobic behavior of the PPO block of the surfactant P123. Since Wanka et al.¹²⁴ showed that significant thermotropic behavior occurs in Pluronics because of changes in the hydrophilicity of the PPO

blocks at around 15-20 °C, for films aged at 4 °C, the "contrast" between hydrophobic PPO and hydrophilic PEO is expected to be small and the polymer may find hydrophilic surfaces to be "neutral". This would be expected to promote orthogonal alignment of the mesophase during low temperature aging. On the other hand, at 23 °C, PPO becomes hydrophobic and the usual contrast mechanisms return. A study of Pluronic F127 [EO₁₀₆PO₇₀EO₁₀₆] in water by FTIR agrees with the conclusion that there is a hydrophilic/hydrophobic transition of PPO somewhere near 20 °C¹³⁹.

To quantify the evolution of thin titania film on modified substrate during aging at 23 °C, the intensity was integrated along the polar coordinate in the detector plane, φ , for $30^\circ < \varphi < 40^\circ$ and over the range of total q from 0-0.1 Å⁻¹. **Figure 9a** shows evolution of the integrated intensity of the diffraction peak vs. time for thin titania film on modified substrate during aging at 23 °C at 13.5 mm above the bottom of the coating or at a set of four other points (averaged). The error bars represent the standard deviation of the intensity of the four points. The intensity changes slowly for the first five minutes, and then increases almost linearly until 15 min of aging. The average intensity of the spots not exposed to repeated x-ray doses is just slightly higher than the intensity at 13.5 mm and the difference is not significant. **Figure 9b** shows the fit of the Avrami equation to the (100) peak intensity data for the thin titania film on modified substrate during aging at 23 °C. A good fit was found for the filled data points, but the unfilled data points did not follow the Avrami equation. The early data (before ~2 minutes) represent an induction period during which formation of the micelles is likely to be occurring but not giving rise to noticeable diffracted intensity. The rate constant k for thin titania film on modified substrate at 23 °C is 0.00388 min⁻². The value of Avrami Index n is 2.0 at 23 °C, which is interpreted as two-dimensional growth with nucleation at the start of the process.¹³⁶⁻¹³⁷ Thus

there is no clear difference in mesostructure growth mechanism for thin films on modified substrates at different aging temperatures. Also, there is no significant difference in the d-spacing for different aging conditions, suggesting that the primary effects of temperature are to change the rate and degree of orientation of the structure. The half-life $t_{1/2}$ calculated from equation 3 for aging at 23 °C comes out to be 13.3 min, which is less than that calculated for thin titania film on modified substrate during aging at 4 °C. This result further indicates that randomly oriented structure allows faster evolution of the mesophase.

The observations made here both confirm the hypothesis that o-HCP films are formed directly by a disorder-order transition for P123-templated films cast onto P123-modified glass slides, and suggest unexpectedly important roles of the environment of the film on the formation of the orthogonally aligned phase. These observations are consistent with modification of the film inducing orthogonal alignment at the substrate/film interface. However, the results also are consistent with orthogonal alignment at the vapor/film interface when the films are aged at 4 °C, and parallel alignment when the films are aged at 23 °C. This leads to the strongest orthogonal alignment when both factors are combined and the films are thin (thin films on modified substrates aged at 4 °C) and random orientation consistent with parallel HCP at the top / orthogonal HCP at the bottom when thin films on modified surfaces are aged at 23 °C. When we compare these results to prior results where the films started aging for a few minutes at 23 °C before being placed in a 4 °C environment, it seems that some degree of parallel micelle alignment may have begun before the films were placed in the refrigerator, which led to a mixed orientation for films on plain glass and fully orthogonal alignment for films on modified substrates. The long TSS observed in the present study helps to explain why orthogonal HCP

mesostructures could be obtained by aging at 4 °C shortly after film formation, with sandwiching of thick films to help reorient random domains that may have started to form initially.

Conclusions

The development of mesostructure and orientation during low temperature aging at 4 °C under high humidity in surfactant-templated titania films was investigated using *in situ* GISAXS. Modification of glass slides with crosslinked template (Pluronic surfactant P123) was used to control surface chemistry to enhance orthogonal orientation of the hexagonal close packed (HCP) mesophase. For a thin (~60 nm) titania film on modified substrate, orthogonally oriented HCP cylindrical micelles start developing after a 7 minute induction period and the intensity evolution followed Avrami kinetics with an index of 2, most likely indicating a mechanism of two dimensional growth of the o-HCP mesophase with nucleation at the start of the process. At the end of the aging period, intense vertical rods due to scattering in the film were observed on both sides of the beam stop, indicating that only the o-HCP phase forms. Unlike prior GISAXS studies based on small molecule surfactant templates,^{52,116-117} no intermediate phase was observed during the development of the o-HCP cylindrical micelles; it formed directly by a disorder-order transition. This observation is consistent with the expected effect of modifying the surface to give an interface equally attractive towards the PEO and PPO blocks of the template, and therefore to reorient the HCP phase orthogonal to the solid substrate. The half-life for o-HCP development in this film after the induction period was about 39.7 min, and led to a well-ordered mesostructure within an hour. Although radiation damage interfered with the GISAXS intensity observed during repeated sampling of a single spot, the intensity recovered when the sampling frequency decreased and was found to be increased in regions of low sampling frequency.

Similar *in situ* GISAXS experiments at 4 °C were performed for three additional samples: thin films on unmodified slides and thicker films (~250 nm) on both modified and unmodified slides. Using plain glass and thicker films were both anticipated to reduce the degree of orthogonal orientation of the HCP phase. Surprisingly, only the o-HCP phase was observed in the GISAXS patterns of all of these samples. No evidence for HCP domains oriented parallel to the substrate or randomly could be found, although the ultimate intensity of these three samples was less than for the thin film on modified substrate (for example, the intensity was about half for the thin film on unmodified substrate than for the modified substrate). The finding of only an o-HCP GISAXS pattern contradicted prior studies which showed randomly oriented HCP patterns for thin films on unmodified substrates⁸⁴ or thick films without sandwiching with a second modified slide.⁸⁵ This was attributed to the low temperature and high relative humidity used from the start of the coating process (in prior studies, films were cast at room temperature and moderate RH prior to being transferred to a refrigerated high RH box for aging). The low temperature (4 °C) is below the temperature where PPO blocks have been shown in previous studies to exhibit a thermotropic shift from hydrophobic (high temperature) behavior to hydrophilic. Also, by analogy with solvent annealing mechanisms of orthogonally orienting HCP block copolymer phases,^{127,133} the high RH may contribute to an orthogonal orientation at the film/vapor interface. For all three samples at 4 °C, a similar Avrami coefficient was found ($n \sim 3$) indicating two-dimensional growth with constant nucleation rate. Thus there is a clear difference in crystal growth mechanism for thin film on modified substrate and other films. Also the induction period was reduced to ~3 min with increased rate of the mesostructure evolution. Also the half-life for thin film on modified substrate is higher than other three films indicating

better orthogonal structure develops slowly. To confirm the temperature effect, aging a thin film sample on a modified substrate at 23 °C was found to lead to randomly oriented HCP channels.

The results obtained here suggest that the most well-defined orthogonally aligned HCP mesophase is obtained by a direct disorder-to-order transition during the transient steady state period after the coating has been deposited. However, the results indicate that aging at low temperature (4 °C) at high RH also contributes substantially to orthogonal orientation of the HCP phase, and that while the order and orientation may not be as complete, these conditions alone can induce partial o-HCP formation for thin films on unmodified slides or thick films. Thus, a temperature below the thermotropic transition temperature of the block copolymer template and a high relative humidity are suggested to be essential to forming orthogonally oriented block copolymer template films, while modifying the substrate for chemical neutrality towards the templating surfactant gives more complete orthogonal orientation across the entirety of the film.

Associated Content

Supporting Information

Representative 2D GISAXS pattern and the corresponding 1D linecut derived by integrating along the q_z direction from 0.025-0.03 \AA^{-1} , evolution of the integrated intensities of the shoulder region, $q_{y,\min} < q_y < q_{y,\max}$, for thin titania film on modified substrate during aging at 4 °C at 13.5 mm above the bottom of the slide and shoulder position as a function of aging time, low magnification (350× magnification) SEM image of titania thin film on modified substrate aged at 4 °C after calcination at 400 °C for 10 minutes using a ramp rate of 25 °C/min, and plan view SEM images of thin titania films near the modified substrate aged at 23 °C and 4 °C after calcination at 400 °C for 10 minutes using a ramp rate of 25 °C/min. This supporting information is available free of charge on the ACS Publications website at <http://pubs.acs.org>.

Author Information

Corresponding Author

* E-mail: stephen.rankin@uky.edu

Notes

The authors declare no competing financial interest.

Acknowledgments

All experiments were performed as part of a U.S. Department of Energy EPSCoR Implementation award supported by grant no. DE-FG02-07-ER46375. The use of the Advanced Photon Source at Argonne National Laboratory for GISAXS measurements was supported by the U. S. Department of Energy, Office of Science, Office of Basic Energy Sciences, under Contract No. DE-AC02-06CH11357. Final data analysis and refinement were completed as part of a NSF EPSCoR research infrastructure award (grant no. IIA-1355438).

References

1. Brinker, C. J.; Lu, Y.; Sellinger, A.; Fan, H., Evaporation-Induced Self-Assembly. Nanostructures Made Easy. *Adv. Mater.* **1999**, *11*, 579-585.
2. Ogawa, M., Formation of Novel Oriented Transparent Films of Layered Silica-Surfactant Nanocomposites. *J. Am. Chem. Soc.* **1994**, *116*, 7941-7942.
3. Ogawa, M., A Simple Set-Gel Route for the Preparation of Silica-Surfactant Mesostructured Materials. *Chem. Comm.* **1996**, 1149-1150.
4. Ogawa, M., Preparation of Transparent Thin Films of Silica-Surfactant Mesostructured Materials. *Supramol. Sci.* **1998**, *5*, 247-251.
5. Lu, Y. G., R.; Drewien, C. A.; Anderson, M. T.; Brinker, C. J.; Gong, W.; Guo, Y.; Soyez, H.; Dunn, B.; Huang, M. H.; Zink, J. I., Continuous Formation of Supported Cubic and Hexagonal Mesoporous Films by Sol-Gel Dip-Coating. *Nature* **1997**, *389*, 364-368.
6. Gulians, V. V.; Carreon, M. A.; Lin, Y. S., Ordered Mesoporous and Macroporous Inorganic Films and Membranes. *J. Membrane Sci.* **2004**, *235*, 53-72.
7. Brinker, C. J.; Dunphy, D. R., Morphological Control of Surfactant-Templated Metal Oxide Films. *Current Opin. Colloid Interface Sci.* **2006**, *11*, 126-132.

8. Yamauchi, Y.; Suzuki, N.; Radhakrishnan, L.; Wang, L., Breakthrough and Future: Nanoscale Controls of Compositions, Morphologies, and Mesochannel Orientations toward Advanced Mesoporous Materials. *Chem. Record* **2009**, *9*, 321-339.
9. Innocenzi, P.; Malfatti, L., Mesoporous Thin Films: Properties and Applications. *Chem. Soc. Rev.* **2013**, *42*, 4198-4216.
10. Faustini, M.; Boissiere, C.; Nicole, L.; Grosso, D., From Chemical Solutions to Inorganic Nanostructured Materials: A Journey into Evaporation-Driven Processes. *Chem. Mat.* **2014**, *26*, 709-723.
11. Li, X.; Song, L.; Vogt, B. D., Tuning Mechanical Properties of Mesoporous Silicas Using Associating Homopolymers/Block Copolymer Blends as Templates. *J. Phys. Chem. C* **2007**, *112*, 53-60.
12. Wang, J.; Cheng, Q.; Tang, Z., Layered Nanocomposites Inspired by the Structure and Mechanical Properties of Nacre. *Chem. Soc. Rev.* **2012**, *41*, 1111-1129.
13. Soler-Illia, G. J. A. A.; Innocenzi, P., Mesoporous Hybrid Thin Films: The Physics and Chemistry Beneath. *Chem. Eur. J.* **2006**, *12*, 4478-4494.
14. Plawsky, J. L.; Kim, J. K.; Schubert, E. F., Engineered Nanoporous and Nanostructured Films. *Mater. Today* **2009**, *12*, 36-45.
15. Volksen, W.; Miller, R. D.; Dubois, G., Low Dielectric Constant Materials. *Chem. Rev.* **2009**, *110*, 56-110.
16. Bearzotti, A.; Bertolo, J. M.; Innocenzi, P.; Falcaro, P.; Traversa, E., Humidity Sensors Based on Mesoporous Silica Thin Films Synthesised by Block Copolymers. *J. Eur. Ceram. Soc.* **2004**, *24*, 1969-1972.
17. Bearzotti, A.; Mio Bertolo, J.; Innocenzi, P.; Falcaro, P.; Traversa, E., Relative Humidity and Alcohol Sensors Based on Mesoporous Silica Thin Films Synthesised from Block Copolymers. *Sensors Actuators B* **2003**, *95*, 107-110.
18. Melde, B.; Johnson, B., Mesoporous Materials in Sensing: Morphology and Functionality at the Meso-Interface. *Anal. Bioanal. Chem.* **2010**, *398*, 1565-1573.
19. Coll, C.; Bernardos, A.; Martínez-Mañez, R.; Sancenón, F., Gated Silica Mesoporous Supports for Controlled Release and Signaling Applications. *Acc. Chem. Res.* **2012**, *46*, 339-349.
20. Wagner, T.; Haffer, S.; Weinberger, C.; Klaus, D.; Tiemann, M., Mesoporous Materials as Gas Sensors. *Chem. Soc. Rev.* **2013**, *42*, 4036-4053.
21. Walcarius, A., Mesoporous Materials and Electrochemistry. *Chem. Soc. Rev.* **2013**, *42*, 4098-4140.
22. Urbanova, V.; Walcarius, A., Vertically-Aligned Mesoporous Silica Films. *Z. Anorg. Allg. Chem.* **2014**, *640*, 537-546.
23. Holmes, J. D.; Spalding, T. R.; Ryan, K. M.; Lyons, D.; Crowley, T.; Morris, M. A., The Use of Templated Mesoporous Materials as Templates for the Development of Ordered Arrangements of Nanowire and Nanorods of Electronically Important Materi. In *Studies in Surface Science and Catalysis*, Sayari, A.; Jaroniec, M., Eds. Elsevier: 2002; Vol. 141, pp 337-344.
24. Ryan, K. M.; Ertz, D.; Olin, H.; Morris, M. A.; Holmes, J. D., Three Dimensional Architectures of Ultra-High Density Semiconducting Nanowires Deposited on Chip. *J. Am. Chem. Soc.* **2003**, *125*, 6284-6288.

25. Wang, D., et al., Electrodeposition of Metallic Nanowire Thin Films Using Mesoporous Silica Templates. *Adv. Mater.* **2003**, *15*, 130-133.
26. Guo, D.-J.; Ding, Y., Porous Nanostructured Metals for Electrocatalysis. *Electroanalysis* **2012**, *24*, 2035-2043.
27. Lee, K.-R.; Kwon, Y.-U., Hard Templates for Fabrication of Nanostructured Films. *Nano* **2010**, *05*, 75-87.
28. Tian, B., et al., Facile Synthesis and Characterization of Novel Mesoporous and Mesorelief Oxides with Gyroidal Structures. *J. Am. Chem. Soc.* **2003**, *126*, 865-875.
29. Yang, H.; Zhao, D., Synthesis of Replica Mesostructures by the Nanocasting Strategy. *J. Mater. Chem.* **2005**, *15*, 1217-1231.
30. Nishiyama, N.; Park, D. H.; Koide, A.; Egashira, Y.; Ueyama, K., A Mesoporous Silica (MCM-48) Membrane: Preparation and Characterization. *J. Membrane Sci.* **2001**, *182*, 235-244.
31. Park, D.-H.; Nishiyama, N.; Egashira, Y.; Ueyama, K., Enhancement of Hydrothermal Stability and Hydrophobicity of a Silica Mcm-48 Membrane by Silylation. *Ind. Eng. Chem. Res.* **2001**, *40*, 6105-6110.
32. Liu, N.; Dunphy, D. R.; Atanassov, P.; Bunge, S. D.; Chen, Z.; López, G. P.; Boyle, T. J.; Brinker, C. J., Photoregulation of Mass Transport through a Photoresponsive Azobenzene-Modified Nanoporous Membrane. *Nano Lett.* **2004**, *4*, 551-554.
33. Brinker, C. J., Evaporation-Induced Self-Assembly: Functional Nanostructures Made Easy. *MRS Bull.* **2004**, *29*, 631-640.
34. Kumar, P.; Gulians, V. V., Periodic Mesoporous Organic-Inorganic Hybrid Materials: Applications in Membrane Separations and Adsorption. *Micropor. Mesopor. Mater.* **2010**, *132*, 1-14.
35. Alonso, B.; Fayon, F.; Massiot, D.; Amenitsch, H.; Malfatti, L.; Kidchob, T.; Costacurta, S.; Innocenzi, P., Hybrid Organic-Inorganic Mesostructured Membranes: Interfaces and Organization at Different Length Scales. *J. Phys. Chem. C* **2010**, *114*, 11730-11740.
36. Chen, Z., et al., DNA Translocation through an Array of Kinked Nanopores. *Nature Mater.* **2010**, *9*, 667-75.
37. Fujita, S.; Koiwai, A.; Kawasumi, M.; Inagaki, S., Enhancement of Proton Transport by High Densification of Sulfonic Acid Groups in Highly Ordered Mesoporous Silica. *Chem. Mater.* **2013**, *25*, 1584-1591.
38. Elbert, J.; Krohm, F.; Rüttiger, C.; Kienle, S.; Didzoleit, H.; Balzer, B. N.; Hugel, T.; Stühn, B.; Gallei, M.; Brunsen, A., Polymer-Modified Mesoporous Silica Thin Films for Redox-Mediated Selective Membrane Gating. *Adv. Func. Mater.* **2014**, *24*, 1591-1601.
39. Islam, S. Z.; Reed, A.; Kim, D. Y.; Rankin, S. E., N₂/Ar Plasma Induced Doping of Ordered Mesoporous TiO₂ Thin Films for Visible Light Active Photocatalysis *Micropor. Mesopor. Mater.* **2015**, *in press*.
40. Liu, Y.-C.; Lu, Y.-F.; Zeng, Y.-Z.; Liao, C.-H.; Chung, J.-C.; Wei, T.-Y., Nanostructured Mesoporous Titanium Dioxide Thin Film Prepared by Sol-Gel Method for Dye-Sensitized Solar Cell. *Int. J. Photoenergy* **2011**, 619069.

41. Vivero-Escoto, J. L.; Chiang, Y. D.; C-Wwu, K.; Yamauchi, Y., Recent Progress in Mesoporous Titania Materials: Adjusting Morphology for Innovative Applications. *Sci. Technol. Adv. Mater.* **2012**, *13*, 013003.
42. Soni, S. S.; Henderson, M. J.; Bardeau, J.-F.; Gibaud, A., Visible-Light Photocatalysis in Titania-Based Mesoporous Thin Films. *Adv. Mater.* **2008**, *20*, 1493-1498.
43. Ismail, A. A.; Bahnemann, D. W., Mesoporous Titania Photocatalysts: Preparation, Characterization and Reaction Mechanisms. *J. Mater. Chem.* **2011**, *21*, 11686-11707.
44. Nakata, K.; Fujishima, A., TiO₂ Photocatalysis: Design and Applications. *J. Photochem. Photobiol. C* **2012**, *13*, 169-189.
45. Pan, J. H.; Zhao, X. S.; Lee, W. I., Block Copolymer-Templated Synthesis of Highly Organized Mesoporous TiO₂-Based Films and Their Photoelectrochemical Applications. *Chem. Eng. J.* **2011**, *170*, 363-380.
46. Zhou, W.; Fu, H. G., Mesoporous TiO₂: Preparation, Doping, and as a Composite for Photocatalysis. *Chemcatchem* **2013**, *5*, 885-894.
47. Hazra, S.; Basu, S., High Sensitivity and Fast Response Hydrogen Sensors Based on Electrochemically Etched Porous Titania Thin Films. *Sensors Actuators B* **2006**, *115*, 403-411.
48. Hagfeldt, A.; Grätzel, M., Light-Induced Redox Reactions in Nanocrystalline Systems. *Chem. Rev.* **1995**, *95*, 49-68.
49. Li, X. S.; Fryxell, G. E.; Birnbaum, J. C.; Wang, C., Effects of Template and Precursor Chemistry on Structure and Properties of Mesoporous TiO₂ Thin Films. *Langmuir* **2004**, *20*, 9095-9102.
50. Jang, K.-S.; Song, M.-G.; Cho, S.-H.; Kim, J.-D., Using the Effects of pH and Moisture to Synthesize Highly Organized Mesoporous Titania Thin Films. *Chem. Commun.* **2004**, 1514-1515.
51. Yu, J. C.; Wang, X.; Fu, X., Pore-Wall Chemistry and Photocatalytic Activity of Mesoporous Titania Molecular Sieve Films. *Chem. Mater.* **2004**, *16*, 1523-1530.
52. Grosso, D.; Soler-Illia, G. J. d. A. A.; Crepaldi, E. L.; Cagnol, F.; Sinturel, C.; Bourgeois, A.; Brunet-Bruneau, A.; Amenitsch, H.; Albouy, P. A.; Sanchez, C., Highly Porous TiO₂ Anatase Optical Thin Films with Cubic Mesostructure Stabilized at 700 °C. *Chem. Mater.* **2003**, *15*, 4562-4570.
53. Villanueva-Cab, J.; Jang, S. R.; Halverson, A. F.; Zhu, K.; Frank, A. J., Trap-Free Transport in Ordered and Disordered TiO₂ Nanostructures. *Nano Lett.* **2014**, *14*, 2305-2309.
54. Jiang, C. H.; Zhang, J. S., Nanoengineering Titania for High Rate Lithium Storage: A Review. *J. Mater. Sci. Technol.* **2013**, *29*, 97-122.
55. Wu, Q. L.; Li, J. C.; Deshpande, R. D.; Subramanian, N.; Rankin, S. E.; Yang, F. Q.; Cheng, Y. T., Aligned TiO₂ Nanotube Arrays as Durable Lithium-Ion Battery Negative Electrodes. *J. Phys. Chem. C* **2012**, *116*, 18669-18677.
56. Lindsay, M. J.; Blackford, M. G.; Attard, D. J.; Luca, V.; Skyllas-Kazacos, M.; Griffith, C. S., Anodic Titania Films as Anode Materials for Lithium Ion Batteries. *Electrochim. Acta* **2007**, *52*, 6401-6411.
57. Lindsay, M. J.; Skyllas-Kazacos, M.; Luca, V., Anodically Synthesized Titania Films for Lithium Batteries: Effect of Titanium Substrate and Surface Treatment. *Electrochim. Acta* **2009**, *54*, 3501-3509.

58. Ortiz, G. F.; Hanzu, I.; Djenizian, T.; Lavela, P.; Tirado, J. L.; Knauth, P., Alternative Li-Ion Battery Electrode Based on Self-Organized Titania Nanotubes. *Chem. Mat.* **2009**, *21*, 63-67.
59. Cauda, V.; Torre, B.; Falqui, A.; Canavese, G.; Stassi, S.; Bein, T.; Pizzi, M., Confinement in Oriented Mesopores Induces Piezoelectric Behavior of Polymeric Nanowires. *Chem. Mat.* **2012**, *24*, 4215-4221.
60. Coakley, K. M.; Srinivasan, B. S.; Ziebarth, J. M.; Goh, C.; Liu, Y. X.; McGehee, M. D., Enhanced Hole Mobility in Regioregular Polythiophene Infiltrated in Straight Nanopores. *Adv. Funct. Mater.* **2005**, *15*, 1927-1932.
61. Cadby, A. J.; Tolbert, S. H., Controlling Optical Properties and Interchain Interactions in Semiconducting Polymers by Encapsulation in Periodic Nanoporous Silicas with Different Pore Sizes. *J. Phys. Chem. B* **2005**, *109*, 17879-17886.
62. Nguyen, T. Q.; Wu, J. J.; Doan, V.; Schwartz, B. J.; Tolbert, S. H., Control of Energy Transfer in Oriented Conjugated Polymer-Mesoporous Silica Composites. *Science* **2000**, *288*, 652-656.
63. Sarker, S.; Mukherjee, B.; Crone, E.; Subramanian, V., Development of a Highly Efficient 1d/0d TiO₂ Nanotube/N-Cdte Photoanode: Single-Step Attachment, Coverage, and Size Control by a Solvothermal Approach. *J. Mater. Chem. A* **2014**, *2*, 4890-4893.
64. Jagannathan, H.; Deal, M.; Nishi, Y.; Kim, H. C.; Freer, E. M.; Sundstrom, L.; Topuria, T.; Rice, P. M., Templated Germanium Nanowire Synthesis Using Oriented Mesoporous Organosilicate Thin Films. *J. Vac. Sci. Technol. B* **2006**, *24*, 2220-2224.
65. Farrell, R. A.; Petkov, N.; Morris, M. A.; Holmes, J. D., Self-Assembled Templates for the Generation of Arrays of 1-Dimensional Nanostructures: From Molecules to Devices. *J. Colloid Interface Sci.* **2010**, *349*, 449-472.
66. Barth, S.; Hernandez-Ramirez, F.; Holmes, J. D.; Romano-Rodriguez, A., Synthesis and Applications of One-Dimensional Semiconductors. *Prog. Mater. Sci.* **2010**, *55*, 563-627.
67. Park, O. H.; Cheng, J. Y.; Hart, M.; Topuria, T.; Rice, P. M.; Krupp, L. E.; Miller, R. D.; Ito, H.; Kim, H. C., High Aspect-Ratio Cylindrical Nanopore Arrays and Their Use for Templating Titania Nanoposts. *Adv. Mater.* **2008**, *20*, 738-742.
68. Yagi, I.; Hayashi, A.; Kimijima, K.; Notsu, H.; Ohta, N.; Yamaguchi, A., Mesoporous Materials toward Nanofabricator and Nanoreactor. *Electrochemistry* **2010**, *78*, 105-113.
69. Gong, D.; Grimes, C. A.; Varghese, O. K.; Hu, W. C.; Singh, R. S.; Chen, Z.; Dickey, E. C., Titanium Oxide Nanotube Arrays Prepared by Anodic Oxidation. *J. Mater. Res.* **2001**, *16*, 3331-3334.
70. Macak, J. M.; Tsuchiya, H.; Ghicov, A.; Yasuda, K.; Hahn, R.; Bauer, S.; Schmuki, P., TiO₂ Nanotubes: Self-Organized Electrochemical Formation, Properties and Applications. *Current Opin. Solid State Mater. Sci.* **2007**, *11*, 3-18.
71. Mor, G. K.; Varghese, O. K.; Paulose, M.; Shankar, K.; Grimes, C. A., A Review on Highly Ordered, Vertically Oriented TiO₂ Nanotube Arrays: Fabrication, Material Properties, and Solar Energy Applications. *Solar Energy Mater. Solar Cells* **2006**, *90*, 2011-2075.
72. Chen, X.; Mao, S. S., Titanium Dioxide Nanomaterials: Synthesis, Properties, Modifications, and Applications. *Chem. Rev.* **2007**, *107*, 2891-2959.

73. Shankar, K.; Basham, J. I.; Allam, N. K.; Varghese, O. K.; Mor, G. K.; Feng, X. J.; Paulose, M.; Seabold, J. A.; Choi, K. S.; Grimes, C. A., Recent Advances in the Use of TiO₂ Nanotube and Nanowire Arrays for Oxidative Photoelectrochemistry. *J. Phys. Chem. C* **2009**, *113*, 6327-6359.
74. Regonini, D.; Bowen, C. R.; Jaroenworarluck, A.; Stevens, R., A Review of Growth Mechanism, Structure and Crystallinity of Anodized TiO₂ Nanotubes. *Mater. Sci. Eng. R* **2013**, *74*, 377-406.
75. Huang, J. Y.; Zhang, K. Q.; Lai, Y. K., Fabrication, Modification, and Emerging Applications of TiO₂ Nanotube Arrays by Electrochemical Synthesis: A Review. *Int. J. Photoenergy* **2013**, 761971.
76. Urade, V. N.; Wei, T. C.; Tate, M. P.; Kowalski, J. D.; Hillhouse, H. W., Nanofabrication of Double-Gyroid Thin Films. *Chem. Mat.* **2007**, *19*, 768-777.
77. Alberius, P. C. A.; Frindell, K. L.; Hayward, R. C.; Kramer, E. J.; Stucky, G. D.; Chmelka, B. F., General Predictive Syntheses of Cubic, Hexagonal, and Lamellar Silica and Titania Mesoporous Thin Films. *Chem. Mater.* **2002**, *14*, 3284-3294.
78. Kellogg, G. J.; Walton, D. G.; Mayes, A. M.; Lambooy, P.; Russell, T. P.; Gallagher, P. D.; Satija, S. K., Observed Surface Energy Effects in Confined Diblock Copolymers. *Phys. Rev. Lett.* **1996**, *76*, 2503-2506.
79. Huang, E.; Pruzinsky, S.; Russell, T. P.; Mays, J.; Hawker, C. J., Neutrality Conditions for Block Copolymer Systems on Random Copolymer Brush Surfaces. *Macromol.* **1999**, *32*, 5299-5303.
80. Huang, E.; Russell, T. P.; Harrison, C.; Chaikin, P. M.; Register, R. A.; Hawker, C. J.; Mays, J., Using Surface Active Random Copolymers to Control the Domain Orientation in Diblock Copolymer Thin Films. *Macromol.* **1998**, *31*, 7641-7650.
81. Thurn-Albrecht, T.; Steiner, R.; DeRouchey, J.; Stafford, C. M.; Huang, E.; Bal, M.; Tuominen, M.; Hawker, C. J.; Russell, T., Nanoscopic Templates from Oriented Block Copolymer Films. *Adv. Mater.* **2000**, *12*, 787-791.
82. Huinink, H. P.; Brokken-Zijp, J. C. M.; van Dijk, M. A.; Sevink, G. J. A., Asymmetric Block Copolymers Confined in a Thin Film. *J. Chem. Phys.* **2000**, *112*, 2452-2462.
83. Pickett, G. T.; Balazs, A. C., Equilibrium Orientation of Confined Diblock Copolymer Films. *Macromol.* **1997**, *30*, 3097-3103.
84. Koganti, V. R.; Dunphy, D.; Gowrishankar, V.; McGehee, M. D.; Li, X.; Wang, J.; Rankin, S. E., Generalized Coating Route to Silica and Titania Films with Orthogonally Tilted Cylindrical Nanopore Arrays. *Nano Lett.* **2006**, *6*, 2567-2570.
85. Das, S.; Wu, Q.; Garlapalli, R. K.; Nagpure, S.; Strzalka, J.; Jiang, Z.; Rankin, S. E., In-Situ Gixsax Investigation of Pore Orientation Effects on the Thermal Transformation Mechanism in Mesoporous Titania Thin Films. *J. Phys. Chem. C* **2013**, *118*, 968-976.
86. Tasinkevych, M.; Ciach, A., Structural Transformations in Confined Lamellar Phases in Oil-Water-Surfactant Mixtures. *J. Chem. Phys.* **2001**, *115*, 8705-8713.
87. Rankin, S. E.; Malanoski, A. P.; Van Swol, F. Monte Carlo Simulation of Amphiphile Self-Assembly During Dip Coating, *Mater. Res. Soc. Symp. Proc.* **2001**, *636*, D121-D126.
88. Richman, E. K.; Brezesinski, T.; Tolbert, S. H., Vertically Oriented Hexagonal Mesoporous Films Formed through Nanometre-Scale Epitaxy. *Nature Mater.* **2008**, *7*, 712-717.
89. Klotz, M.; Albouy, P.-A.; Ayrat, A.; Ménager, C.; Grosso, D.; Van der Lee, A.; Cabuil, V.; Babonneau, F.; Guizard, C., The True Structure of Hexagonal Mesophase-Templated Silica Films

- as Revealed by X-Ray Scattering: Effects of Thermal Treatments and of Nanoparticle Seeding. *Chem. Mater.* **2000**, *12*, 1721-1728.
90. Grosso, D.; Balkenende, A. R.; Albouy, P. A.; Ayril, A.; Amenitsch, H.; Babonneau, F., Two-Dimensional Hexagonal Mesoporous Silica Thin Films Prepared from Block Copolymers: Detailed Characterization and Formation Mechanism. *Chem. Mater.* **2001**, *13*, 1848-1856.
 91. Grosso, D.; Babonneau, F.; Albouy, P.-A.; Amenitsch, H.; Balkenende, A. R.; Brunet-Bruneau, A.; Rivory, J., An in Situ Study of Mesostructured CTAB-Silica Film Formation During Dip Coating Using Time-Resolved SAXS and Interferometry Measurements. *Chem. Mater.* **2002**, *14*, 931-939.
 92. Doshi, D. A.; Gibaud, A.; Goletto, V.; Lu, M.; Gerung, H.; Ocko, B.; Han, S. M.; Brinker, C. J., Peering into the Self-Assembly of Surfactant Templated Thin-Film Silica Mesophases. *J. Am. Chem. Soc.* **2003**, *125*, 11646-11655.
 93. Gibaud, A.; Grosso, D.; Smarsly, B.; Baptiste, A.; Bardeau, J. F.; Babonneau, F.; Doshi, D. A.; Chen, Z.; Brinker, C. J.; Sanchez, C., Evaporation-Controlled Self-Assembly of Silica Surfactant Mesophases. *J. Phys. Chem. B* **2003**, *107*, 6114-6118.
 94. Grosso, D.; Babonneau, F.; Sanchez, C.; de A.A. Soler-Illia, G. J.; Crepaldi, E. L.; Albouy, P. A.; Amenitsch, H.; Balkenende, A. R.; Brunet-Bruneau, A., A First Insight in the Mechanisms Involved in the Self-Assembly of 2D-Hexagonal Templated SiO₂ and TiO₂ Mesostructured Films During Dip-Coating. *J. Sol-Gel Sci. Technol.* **2003**, *26*, 561-565.
 95. Grosso, D.; Cagnol, F.; Soler-Illia, G. J. d. A. A.; Crepaldi, E. L.; Amenitsch, H.; Brunet-Bruneau, A.; Bourgeois, A.; Sanchez, C., Fundamentals of Mesostructuring through Evaporation-Induced Self-Assembly. *Adv. Func. Mater.* **2004**, *14*, 309-322.
 96. Innocenzi, P.; Malfatti, L.; Kidchob, T.; Costacurta, S.; Falcaro, P.; Piccinini, M.; Marcelli, A.; Morini, P.; Sali, D.; Amenitsch, H., Time-Resolved Simultaneous Detection of Structural and Chemical Changes During Self-Assembly of Mesostructured Films. *J. Phys. Chem. C* **2007**, *111*, 5345-5350.
 97. Grosso, D.; Ribot, F.; Boissiere, C.; Sanchez, C., Molecular and Supramolecular Dynamics of Hybrid Organic-Inorganic Interfaces for the Rational Construction of Advanced Hybrid Nanomaterials. *Chem. Soc. Rev.* **2011**, *40*, 829-48.
 98. Innocenzi, P.; Malfatti, L.; Kidchob, T.; Falcaro, P.; Costacurta, S.; Guglielmi, M.; Mattei, G.; Bello, V.; Amenitsch, H., Thermal-Induced Phase Transitions in Self-Assembled Mesostructured Films Studied by Small-Angle X-Ray Scattering. *J. Synchrotron Rad.* **2005**, *12*, 734-8.
 99. Innocenzi, P.; Kidchob, T.; Bertolo, J. M.; Piccinini, M.; Guidi, M. C.; Marcelli, C., Time-Resolved Infrared Spectroscopy as an in Situ Tool to Study the Kinetics During Self-Assembly of Mesostructured Films. *J. Phys. Chem. B* **2006**, *110*, 10837-10841.
 100. Innocenzi, P.; Malfatti, L.; Kidchob, T.; Grosso, D., Controlling the Processing of Mesoporous Titania Films by in Situ Ftir Spectroscopy: Getting Crystalline Micelles into the Mesopores. *J. Phys. Chem. C* **2010**, *114*, 10806-10811.
 101. Flodström, K.; Teixeira, C. V.; Amenitsch, H.; Alfredsson, V.; Lindén, M., In Situ Synchrotron Small-Angle X-Ray Scattering/X-Ray Diffraction Study of the Formation of SBA-15 Mesoporous Silica. *Langmuir* **2004**, *20*, 4885-4891.
 102. Grosso, D.; Babonneau, F.; Soler-Illia, G. J. d. A. A.; Albouy, P.-A.; Amenitsch, H., Phase Transformation During Cubic Mesostructured Silica Film Formation. *Chem. Commun.* **2002**, 748-749.

103. Koganti, V. R.; Rankin, S. E., Synthesis of Surfactant-Templated Silica Films with Orthogonally Aligned Hexagonal Mesophase. *J. Phys. Chem. B* **2005**, *109*, 3279-3283.
104. Gibaud, A.; Dourdain, S.; Gang, O.; Ocko, B. M., In Situ Grazing Incidence Small-Angle X-Ray Scattering Real-Time Monitoring of the Role of Humidity During the Structural Formation of Templated Silica Thin Films. *Phys. Rev. B* **2004**, *70*, 4.
105. Cagnol, F. G., D.; Soler-Illia, G. J.; Crepaldi, E. L.; Babonneau, F.; Amenitsch, H.; Sanchez, C., Humidity-Controlled Mesostructuration in CTAB-Templated Silica Thin Film Processing. The Existence of a Modulable Steady State. *J. Mater. Chem.* **2003**, *13*, 61-66.
106. Urade, V. N.; Bollmann, L.; Kowalski, J. D.; Tate, M. P.; Hillhouse, H. W., Controlling Interfacial Curvature in Nanoporous Silica Films Formed by Evaporation-Induced Self-Assembly from Nonionic Surfactants. II. Effect of Processing Parameters on Film Structure. *Langmuir* **2007**, *23*, 4268-4278.
107. Besson, S.; Gacoin, T.; Ricolleau, C.; Jacquiod, C.; Boilot, J. P., Phase Diagram for Mesoporous CTAB-Silica Films Prepared under Dynamic Conditions. *J. Mater. Chem.* **2003**, *13*, 404-409.
108. Boudot, M.; Gaud, V.; Louarn, M.; Selmane, M.; Grosso, D., Sol-Gel Based Hydrophobic Antireflective Coatings on Organic Substrates: A Detailed Investigation of Ammonia Vapor Treatment (AVT). *Chem. Mater.* **2014**, *26*, 1822-1833.
109. Grosso, D.; Balkende, A. R.; Albouy, P. A.; Ayrat, A.; Amentisch, H.; Babonneau, F., Two-Dimensional Hexagonal Mesoporous Silica Thin Films Prepared from Block Copolymers: Detailed Characterization and Formation Mechanism. *Chem. Mater.* **2001**, *13*, 1848-1856.
110. Collard, X.; Van der Schueren, B.; Rooke, J. C.; Aprile, C.; Su, B. L., A Comprehensive Study of the Reaction Parameters Involved in the Synthesis of Silica Thin Films with Well-Ordered Unidirectional Mesopores. *J. Colloid Interface Sci.* **2013**, *401*, 23-33.
111. Lee, Y.-F.; Chang, K.-H.; Chu, C.-Y.; Chen, H.-L.; Hu, C.-C., Microstructure Tuning of Mesoporous Silica Prepared by Evaporation-Induced Self-Assembly Processes: Interactions among Solvent Evaporation, Micelle Formation/Packing and Sol Condensation. *RSC Adv.* **2011**, *1*, 401-407.
112. Keller, A.; Segal-Peretz, T.; Kauffmann, Y.; Frey, G. L., Control over in-Channel Mesostructure Orientation through Aam Surface Modification. *Phys. Chem. Chem. Phys.* **2013**, *15*, 13637-13645.
113. Platschek, B.; Keilbach, A.; Bein, T., Mesoporous Structures Confined in Anodic Alumina Membranes. *Adv. Mater.* **2011**, *23*, 2395-2412.
114. Stein, A.; Rudisill, S. G.; Petkovich, N. D., Perspective on the Influence of Interactions between Hard and Soft Templates and Precursors on Morphology of Hierarchically Structured Porous Materials. *Chem. Mat.* **2014**, *26*, 259-276.
115. Cagnol, F.; Grosso, D.; Soler-Illia, G. J. d. A. A.; Crepaldi, E. L.; Babonneau, F.; Amenitsch, H.; Sanchez, C., Humidity-Controlled Mesostructuration in CTAB-Templated Silica Thin Film Processing. The Existence of a Modulable Steady State. *J. Mater. Chem.* **2003**, *13*, 61-66.
116. Koh, C. W.; Lee, U. H.; Song, J. K.; Lee, H. R.; Kim, M. H.; Suh, M.; Kwon, Y. U., Mesoporous Titania Thin Film with Highly Ordered and Fully Accessible Vertical Pores and Crystalline Walls. *Chem. Asian J.* **2008**, *3*, 862-867.

117. Ko, Y. S.; Koh, C. W.; Lee, U. H.; Kwon, Y. U., Synthesis of Mesoporous Titania Thin Films with Vertical Pore Channels and Thick and Crystalline Walls. *Micropor. Mesopor. Mater.* **2011**, *145*, 141-145.
118. Jiang, Z.; Li, X.; Strzalka, J.; Sprung, M.; Sun, T.; Sandy, A. R.; Narayanan, S.; Lee, D. R.; Wang, J., The Dedicated High-Resolution Grazing-Incidence X-Ray Scattering Beamline 8-Id-E at the Advanced Photon Source. *J. Synchrotron Rad.* **2012**, *19*, 627-636.
119. Jiang, Z., Gisxgui: A Matlab Toolbox for Grazing-Incidence X-Ray Scattering Data Visualization and Reduction, and Indexing of Buried Three-Dimensional Periodic Nanostructured Films. *J. Appl. Crystallogr.* **2015**, *48*, 917-926.
120. Smilgies, D. M., Scherrer Grain-Size Analysis Adapted to Grazing-Incidence Scattering with Area Detectors. *J. Appl. Crystallogr.* **2009**, *42*, 1030-1034.
121. Koganti, V. R.; Das, S.; Rankin, S. E., In Situ FTIR Investigation of the Kinetics of Silica Polycondensation in Surfactant Templated, Mesostructured Thin Films. *J. Phys. Chem. C* **2014**, *118*, 19450-19461.
122. Kim, S. H.; Misner, M. J.; Xu, T.; Kimura, M.; Russell, T. P., Highly Oriented and Ordered Arrays from Block Copolymers Via Solvent Evaporation. *Adv. Mater.* **2004**, *16*, 226-231.
123. Maret, M., et al., Probing Self-Assembly of Cylindrical Morphology Block Copolymer Using in Situ and Ex Situ Grazing Incidence Small-Angle X-Ray Scattering: The Attractive Case of Graphoepitaxy. *Macromol.* **2014**, *47*, 7221-7229.
124. Wanka, G.; Hoffmann, H.; Ulbricht, W., Phase Diagrams and Aggregation Behavior of Poly(Oxyethylene)-Poly(Oxypropylene)-Poly(Oxyethylene) Triblock Copolymers in Aqueous Solutions. *Macromol.* **1994**, *27*, 4145-4159.
125. Malfatti, L.; Kidchob, T.; Costacurta, S.; Falcaro, P.; Schiavuta, P.; Amenitsch, H.; Innocenzi, P., Highly Ordered Self-Assembled Mesostructured Hafnia Thin Films: An Example of Rewritable Mesostructure. *Chem. Mater.* **2006**, *18*, 4553-4560.
126. Kothari, R.; Winter, H. H.; Watkins, J. J., Rheological Study of Order-to-Disorder Transitions and Phase Behavior of Block Copolymer-Surfactant Complexes Containing Hydrogen-Bonded Small Molecule Additives. *Macromol.* **2014**, *47*, 8048-8055.
127. Paradiso, S. P.; Delaney, K. T.; Garcia-Cervera, C. J.; Ceniceros, H. D.; Fredrickson, G. H., Block Copolymer Self Assembly During Rapid Solvent Evaporation: Insights into Cylinder Growth and Stability. *ACS Macro Lett.* **2014**, *3*, 16-20.
128. Phillip, W. A.; Hillmyer, M. A.; Cussler, E. L., Cylinder Orientation Mechanism in Block Copolymer Thin Films Upon Solvent Evaporation. *Macromol.* **2010**, *43*, 7763-7770.
129. Kolmogorov, A., A Statistical Theory for the Recrystallization of Metals. *Akad. nauk SSSR, Izv., Ser. Matem* **1937**, *1*.
130. Avrami, M., Kinetics of Phase Change. I. General Theory. *J. Chem. Phys.* **1939**, *7*, 1103-1112.
131. Avrami, M., Kinetics of Phase Change. II. Transformation-Time Relations for Random Distribution of Nuclei. *J. Chem. Phys.* **1940**, *8*, 212-224.
132. Avrami, M., Granulation, Phase Change, and Microstructure Kinetics of Phase Change. III. *J. Chem. Phys.* **1941**, *9*, 177-184.
133. Jena, A. K., Chaturvedi, M. C., *Phase Transformations in Materials*. Prentice Hall, 1992.

134. Zhao, Y.; Chen, X.; Yang, C.; Zhang, G., Mesoscopic Simulation on Phase Behavior of Pluronic P123 Aqueous Solution. *J. Phys. Chem. B* **2007**, *111*, 13937-13942.
135. Lund, R.; Willner, L.; Richter, D., Kinetics of Block Copolymer Micelles Studied by Small-Angle Scattering Methods. *Adv. Polym Sci.* **2013**, *259*, 51-158.
136. Ding, Z.; Spruiell, J. E., Interpretation of the Nonisothermal Crystallization Kinetics of Polypropylene Using a Power Law Nucleation Rate Function. *J. Polym. Sci. B* **1997**, *35*, 1077-1093.
137. Toro-Vazquez, J.; Dibildox-Alvarado, E.; Charó-Alonso, M.; Herrera-Coronado, V.; Gómez-Aldapa, C., The Avrami Index and the Fractal Dimension in Vegetable Oil Crystallization. *J. Am. Oil Chem. Soc.* **2002**, *79*, 855-866.
138. Lyakhova, K. S.; Sevink, G. J. A.; Zvelindovsky, A. V.; Horvat, A.; Magerle, R., Role of Dissimilar Interfaces in Thin Films of Cylinder-Forming Block Copolymers. *J. Chem. Phys.* **2004**, *120*, 1127-1137.
139. Su, Y.-l.; Wang, J.; Liu, H.-z., FTIR Spectroscopic Investigation of Effects of Temperature and Concentration on PEO-PPO-PEO Block Copolymer Properties in Aqueous Solutions. *Macromol.* **2002**, *35*, 6426-6431.

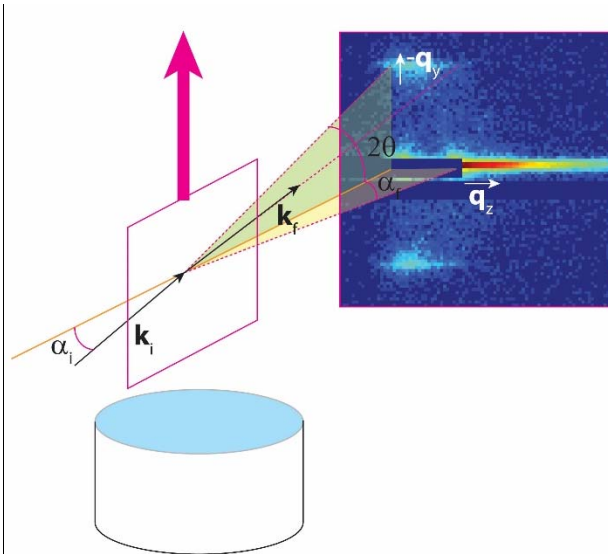


Figure 1. Scattering geometry for *in situ* dip coating GISAXS measurements. For each experiment, a vertically oriented sample slide is raised from a reservoir at a controlled rate. X-rays are incident on the sample at an angle α_i and specularly reflected at angle α_f in the horizontal plane, normal to the plane of the sample. The projection of the scattering angle onto the vertical plane is 2θ , and the wave-vector transfer components q_z and q_y are perpendicular and parallel to the sample plane, respectively.

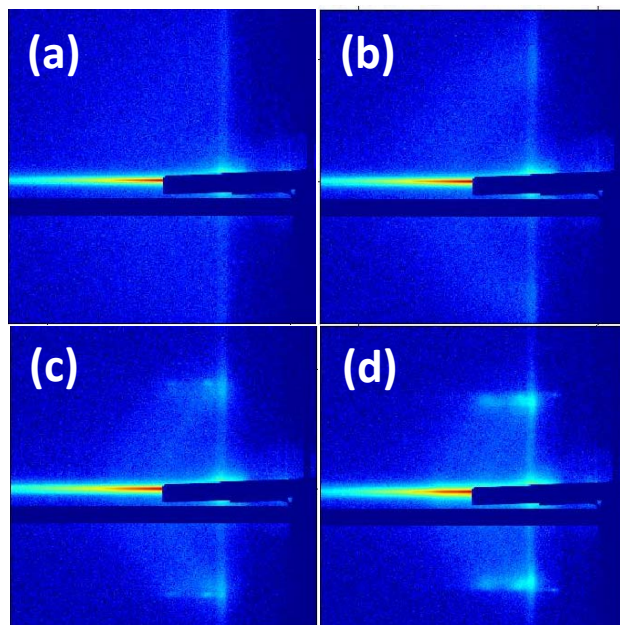


Figure 2. 2D GISAXS patterns showing the evolution of mesostructure for thin (~60 nm thick) titania film on modified substrate after aging at 4 °C and ~80% RH for a) 10 min b) 15 min c) 20 min and d) 75 min after coating.

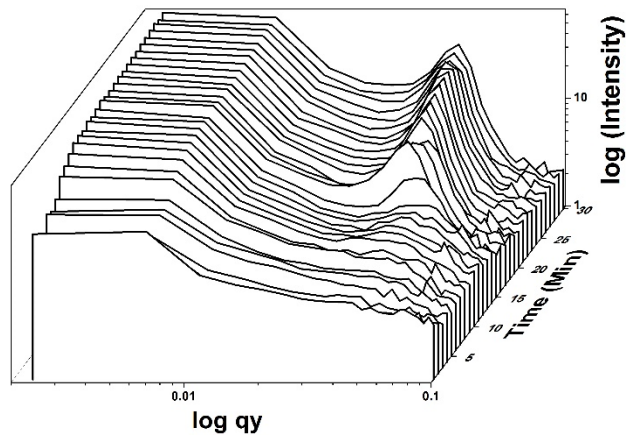


Figure 3. Waterfall plot showing the evolution of the mesostructure for thin titania film on modified substrate during aging 4 °C for the first 30 minutes. The plots were generated by integrating slices from the 2D GISAXS patterns for q_z values from 0.025 to 0.03 \AA^{-1} .

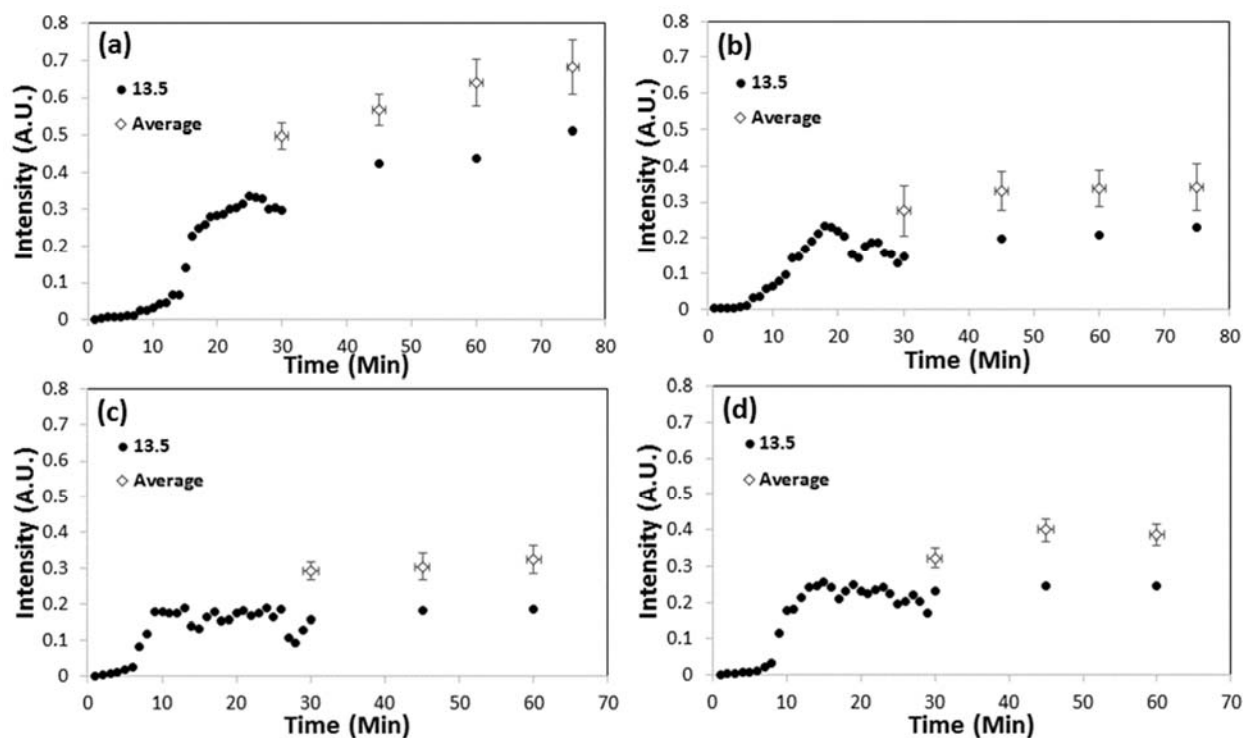


Figure 4. Evolution of the integrated intensities of the (100) peak of the o-HCP structure vs. time for (a) thin titania film on modified substrate, (b) thin titania film on unmodified substrate, (c) thick titania film on modified substrate, and (d) thick titania film on unmodified substrate during aging at 4 °C at 13.5 mm above the bottom of the coating or at a set of four other points (averaged). The error bars represent the standard deviation of the intensity of the four points excluding the measurement at 13.5 mm.

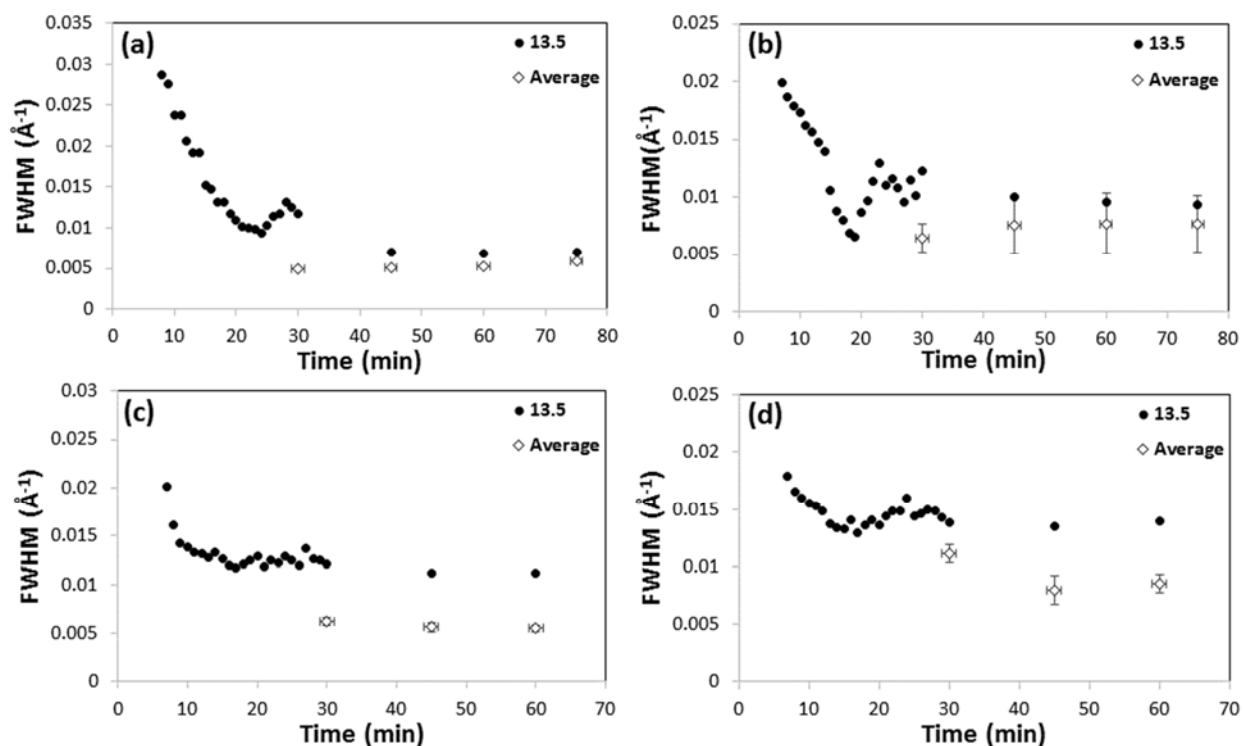


Figure 5. FWHM (full width at half maximum) for (a) thin titania film on modified substrate, (b) thin titania film on unmodified substrate, (c) thick titania film on modified substrate, and (d) thick titania film on unmodified substrate at 13.5 mm above the bottom of the coating or at a set of four other points (averaged). The error bars represent the standard deviation of the FWHM of the four points excluding the measurement at 13.5 mm.

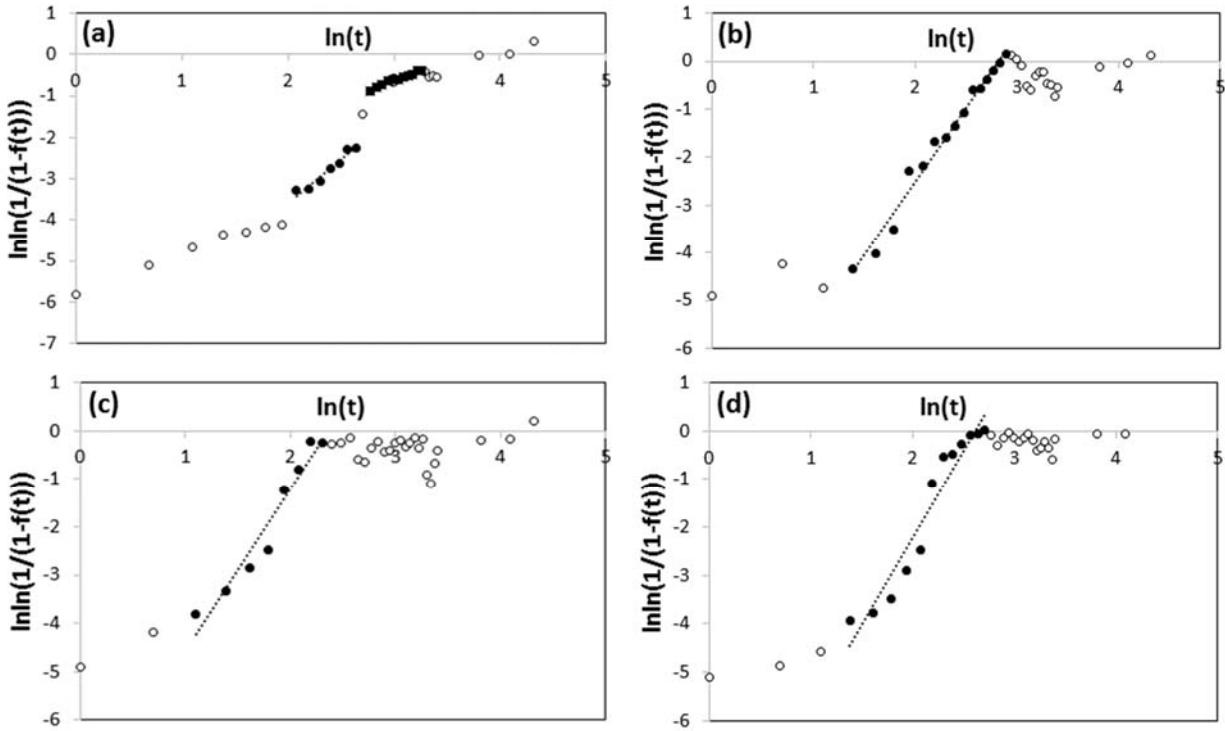


Figure 6. The linearized Avrami equation fit to data for (a) thin titania film on modified substrate, (b) thin titania film on unmodified substrate, (c) thick titania film on modified substrate, and (d) thick titania film on unmodified substrate during aging at 4 °C. The filled symbols were fit and the open symbols were not, either because they were measured during the induction period (for early data) or because they were measured after significant radiation damage was observed (for late data).

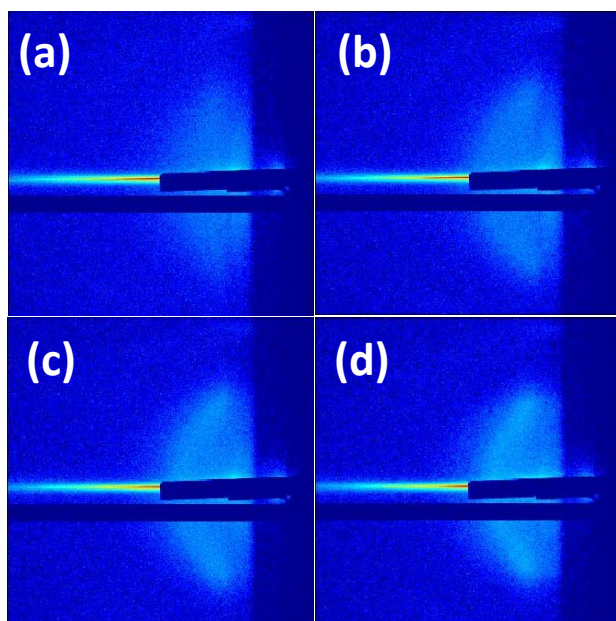


Figure 7. Selected representative 2D GISAXS patterns collected during the aging of a thin P123-templated titania film on a modified substrate during aging at 23 °C for aging times of (a) 5 min, (b) 8 min, (c) 10 min and (d) 15 min.

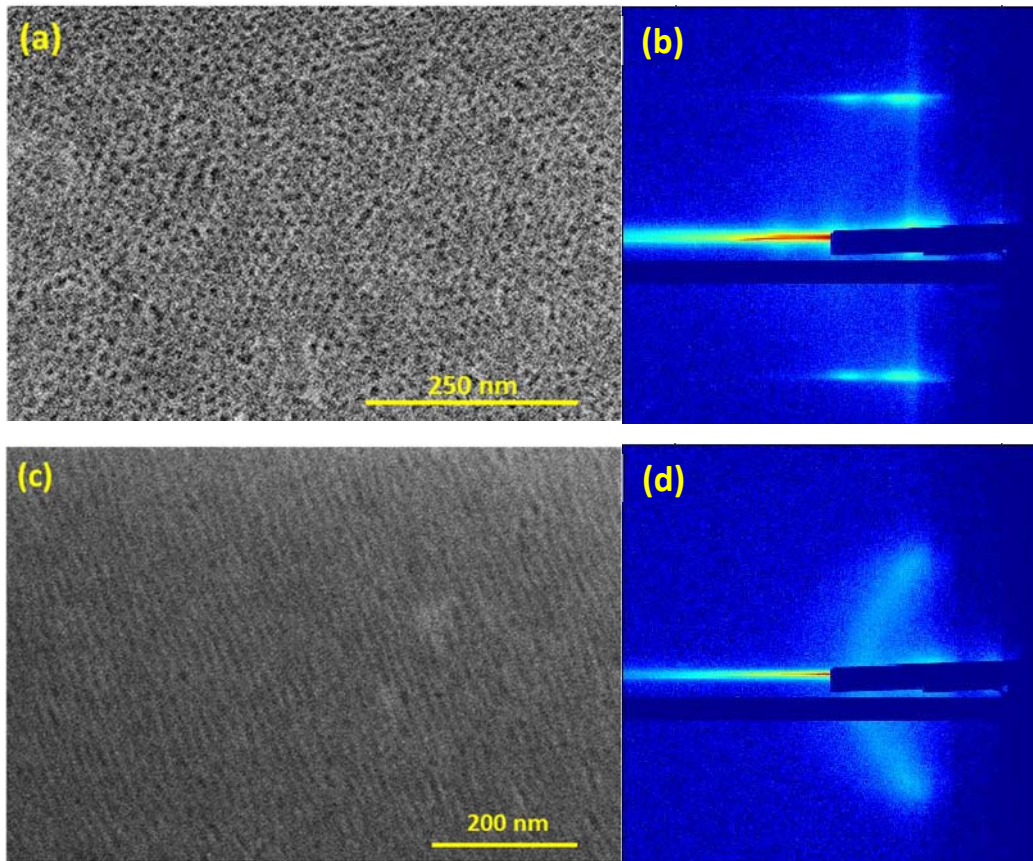


Figure 8. Top view SEM images of thin titania films on modified substrate aged at (a) 4 °C and (c) 23 °C after calcination at 400 °C for 10 minutes using a ramp rate of 25 °C/min; and GISAXS patterns after 30 minutes of aging at (b) 4 °C or (d) 23° C.

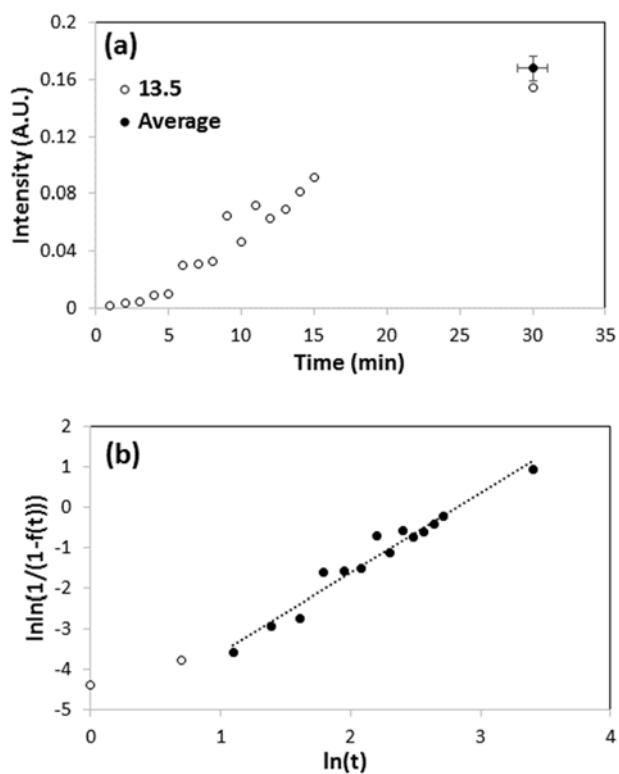
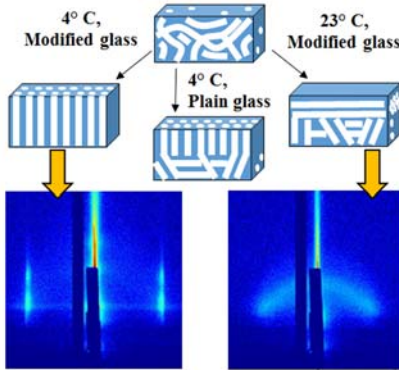


Figure 9. (a) Evolution of the integrated intensity of the diffraction peak vs. time for thin titania film on modified substrate during aging at 23 °C at a point 13.5 mm above the bottom of the coating or at a set of four other points (averaged). The error bars represent the standard deviation of the intensity of the four points excluding the measurement at 13.5 mm. (b) The linearized Avrami equation fit to data for thin film on modified substrate during aging at 23 °C. The filled symbols were fit and the open symbols were not, because they were measured during the induction period (Induction period = 2 min, Avrami parameters, $n = 2.0$, $k = 0.00388 \text{ min}^{-2}$).

Table 1. Parameters found by fitting the Avrami equation to each of the films aged at 4 °C and high relative humidity.

Sample	Maximum Average Intensity (A.U.)	Induction Time (min)	<i>n</i>	k (min⁻ⁿ)	Half Life (min)
Thin film on modified substrate	0.68± 0.073	7	2.07 ± 0.22	0.00044	39.7
			0.97 ± 0.05	0.028	24.7
Thin film on unmodified substrate	0.34± 0.066	3	3.08 ± 0.11	0.00017	14.8
Thick film on modified substrate	0.32± 0.038	2	3.33 ± 0.32	0.00038	9.5
Thick film on unmodified substrate	0.40± 0.030	3	3.63 ± 0.30	0.000075	12.3

Table of Contents Graphic



Supporting Information

***In Situ* GISAXS Investigation of Low-Temperature Aging in Oriented Surfactant-Mesostructured Titania Thin Films**

*Suraj Nagpure[†], Saikat Das[†], Ravinder K. Garlapalli[†], Joseph Strzalka[‡],
and Stephen E. Rankin^{†,*}*

[†] University of Kentucky, Chemical & Materials Engineering Department, 177 F.P. Anderson Tower, Lexington, KY 40506-0046 USA

[‡] X-Ray Science Division, Argonne National Laboratory, Argonne, IL, USA

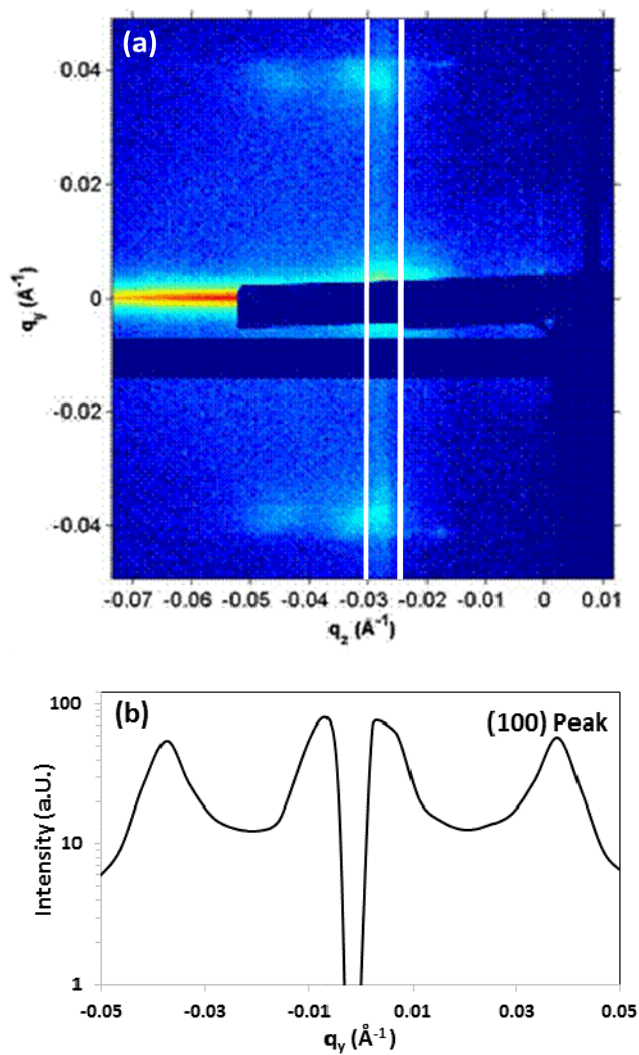


Figure S11. (a) Representative 2D GISAXS pattern with the region used for linecuts shown by vertical white lines, and (b) the corresponding 1D linecut derived by integrating along the q_z direction from 0.025-0.03 Å⁻¹.

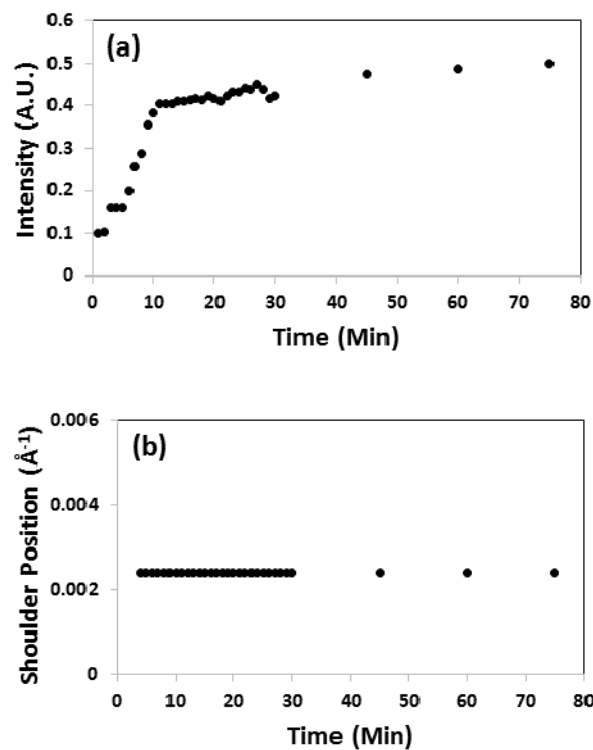


Figure SI2. (a) Evolution of the integrated intensities of the shoulder region near the beamstop, $q_{y,\min} < q_y < q_{y,\max}$, for the thin titania film on modified substrate during aging at 4 °C at 13.5 mm above the bottom of the slide and (b) position of the maximum in the shoulder ($q_{y,\max}$) as a function of aging time

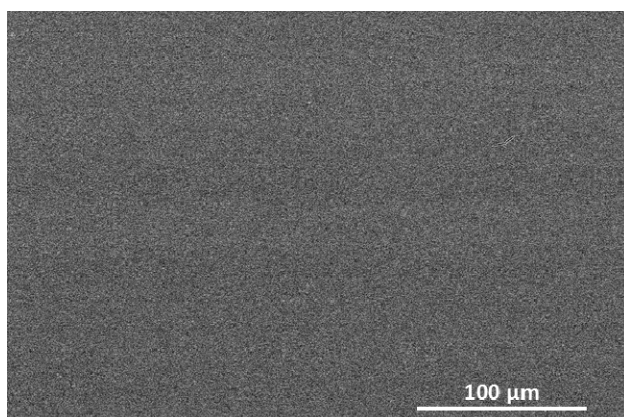


Figure S13. Low magnification (350× magnification) SEM image of a thin titania film on modified substrate aged at 4 °C after calcination at 400 °C for 10 minutes using a ramp rate of 25 °C/min. No cracks or defects can be seen, indicating that the adhesion of the titania film is not affected by the removal of the crosslinked P123 layer during calcination.

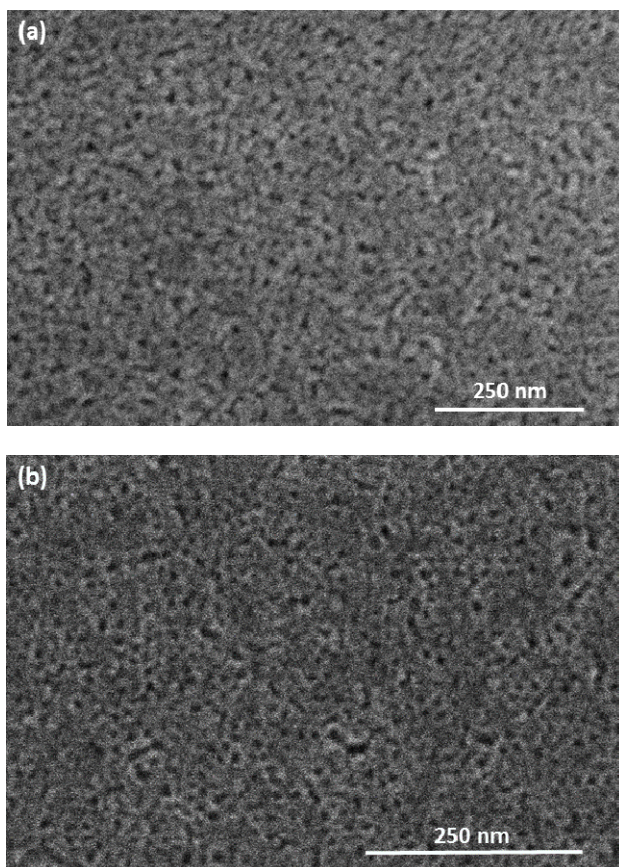


Figure SI4. Plan view SEM images of thin titania films at the film/substrate interface for films cast onto modified substrates, aged at (a) 23 °C and (b) 4 °C and calcined at 400 °C for 10 minutes using a ramp rate of 25 °C/min. These images were obtained by placing a piece of masking tape onto one side of the glass slide prior to processing and then peeling off the tape, flipping it and remounting on a new glass slide. Removal of the masking tape during calcination revealed the structure shown here.